evoked by microinjection of glutamate with or without preinjection of Y-27632 into the NTS of rats. Furthermore, in medulla slice preparations, we recorded single-unit activity of NTS neurons evoked by extracellular iontophoretic application of NMDA or α-amino-3-hydroxy-5-methyl-4-isoxazolepropionate (AMPA) before and after Y-27632 perfusion.

Methods

This study was reviewed and approved by the committee on ethics of animal experiments, Kyushu University Graduate School of Medical Sciences, and was conducted according to the guidelines for animal experiments of Kyushu University. Male WKY or SHR (280 to 340 g; 16 to 20 weeks old) were used in the present study. Rats were obtained from an established colony at the Animal Research Institute of Kyushu University Faculty of Medicine (Fukuoka, Japan).

Microinjection Study

Animals were anesthetized with sodium pentobarbital (50 mg/kg IP; followed by 10 to 20 mg/kg per hour IV), and a catheter was inserted into the right femoral artery for measurement of arterial pressure and HR and into the femoral vein for infusion of pentobarbital. The anesthetized animals were artificially ventilated and placed in a stereotaxic frame. The dorsal surface of the medulla was exposed, and the microinjection sites were defined according to a rat brain atlas:[16] the coordinates for the NTS were 0.6 mm rostral and 0.6 mm lateral to the calamus scriptorius and 0.5 mm below the dorsal surface of the medulla, as described previously.[17] Microinjection was performed with a micropipette connected to a Hamilton microsyringe. We used 3 doses of glutamate (2 pmol, 20 pmol, and 200 pmol; 0.1, 1.0, and 10 mmol/L in 20 nL, injected over a 5-s period) and tested 1 or 2 doses of glutamate in each rat. To test 2 doses of glutamate in 1 rat, we microinjected the lower dose first. More than 30 minutes after the microinjection of lower dose of glutamate, we replaced the pipette using the same coordinates, and then the higher dose of glutamate was microinjected into the NTS. In a preliminary study, we observed a similar depressor response to glutamate microinjected into the NTS using 2 separate pipettes with equal doses of glutamate. Care was taken to maintain stable arterial blood pressure and HR during the experiment. In the Y-27632 coinjection study, we used a 2-barrel micropipette. One side of the pipette was filled with glutamate and the other side with Y-27632 (40 pmol; 0.5 mmol/L in 80 nL, injected over a 20-s period) or vehicle (artificial cerebrospinal fluid [a-CSF]; 80 nL, injected over a 20-s period). First, we microinjected only glutamate and waited ≥30 minutes as in the single-barrel pipette experiments, and then Y-27632 (or a-CSF) and glutamate were injected. Because the glutamate response was rapid and of short duration, we microinjected glutamate into the NTS unilaterally 60 s after the Y-27632 or a-CSF injection. In addition, to avoid the possibility of differences in the amount of drug spread, a microdialysis probe with an external injection line (MI-A-I-12-01; Eicom) connected to a syringe pump was placed unilaterally into the NTS. We confirmed previously that the dialysis probe was permeable to NMDA.[18] Therefore, NMDA (0.5 mmol/L; infusion speed 2 μL/min for 5 minutes) was infused through a microdialysis probe and Y-27632 (5 mmol/L; injection speed 0.02 μL/min for 5 minutes) was injected through the injection line with syringe pumps.[18] We selected the dose of NMDA or Y-27632 to produce an arterial pressure reduction of the same magnitude as that produced by 2.0 to 20 pmol glutamate microinjection or 0.5 mmol/L Y-27632 microinjection into the NTS.

Single-Unit Recordings of NTS Neurons

We performed single-unit recordings of NTS neurons as described previously.[19–21] Under ether anesthesia, the rat was killed by cervical dislocation, and the brain stem was rapidly removed and placed in cold Krebs–Ringer solution containing 126 mmol/L NaCl, 5 mmol/L KCl, 2.4 mmol/L $CaCl_2$, 1.3 mmol/L $MgSO_4$, 1.26 mmol/L KH_2PO_4, 26 mmol/L $NaHCO_3$, and 10 mmol/L D-glucose, saturated with 95% O_2 and 5% CO_2. A horizontal brain stem slice (400-μm thick) containing the area postrema and NTS was obtained using a vibratome (DTK-1000; Dosaka). The slice was incubated for ≥2 hours in Krebs–Ringer solution bubbled with 95% O_2 and 5%CO_2 before starting the experiment. The recording chamber was perfused with oxygenated Krebs–Ringer solution at 34°C. Slices were placed on a Plexiglas mesh in a submerged recording chamber and covered with nylon mesh and a silver ring to support the tissue. The recording chamber was perfused with oxygenated Krebs–Ringer solution at a flow rate of 3 mL/min. Using a microscope, the NTS was visualized as a translucent area in the slice, and the electrode was advanced into the NTS until an action potential was recorded. The spikes were amplified (MWZ-7200 and MEG-1200; Nihon-Koden), and the raw neurogram and firing rate were displayed on an oscilloscope (DS-8605; Iwatsu) and recorded; the output was fed into a computer program Chart 4 (AD Instruments) to calculate the numbers of spikes per second. NMDA or AMPA was injected using a 2-barrel glass electrode, which was independent of the recording electrode. The most effective infusion field was a circular area ≈50 μm in diameter.[22] The iontophoretic system was a Neurophore model BH-2 control unit (Medical Systems), and the chemicals were prepared as follows: NMDA (50 mmol/L in distilled water, pH 7.5) and AMPA (10 mmol/L in 150 mmol/L NaCl, pH 7.5). The current used (1000-ms duration) was −5 to −30 nA for the NMDA pipette and −5 to −20 nA for the AMPA pipette. Retention current was not routinely applied. For NMDA and AMPA, the current was varied for each neuron because of the variations in electrodes and ejection sites, and then currents were adjusted to produce almost identical responses for NMDA and AMPA. The control firing rate in spikes per second (Hz) induced by NMDA or AMPA was recorded before and after Y-27632 perfusion. Y-27632 (50 μmol/L) was dissolved in oxygenated Krebs–Ringer solution and perfused at a flow rate of 3 mL/min for 6 minutes. The effects of Y-27632 were defined as the peak changes in spikes per second between before and after Y-27632 perfusion.

Statistical Analysis

All values are expressed as mean±SE. Two-way ANOVA was used to compare the responses of glutamate injection in each dose between WKY and SHR and the effects of Y-27632 on the responses to glutamate injection for each dose. Any 2 mean values were compared by application of the Bonferroni correction for multiple comparisons. Differences were considered to be statistically significant at a P value of <0.05.

Results

Baseline Characteristics

Baseline mean arterial pressure (MAP) and HR in each group are shown in the Table. MAP and HR were significantly higher in SHR than in WKY. Unilateral injection of Y-27632 induced a decrease in MAP and HR in SHR but not in WKY (Table).

Effects of Rho-Kinase Inhibition on Glutamate Sensitivity in the NTS

Unilateral microinjection of glutamate into the NTS decreased MAP in a dose-dependent manner in WKY and SHR (Figure 1). When lower doses of glutamate were microinjected, the magnitude of the decrease in MAP was significantly reduced in SHR compared with WKY (Figure 1). The percent change in MAP was significantly greater in WKY than in SHR for all doses of glutamate examined (Figure 1). The magnitude of the decrease in HR induced by glutamate injection did not differ between WKY and SHR (Figure 1). The magnitude of the MAP decrease evoked by unilateral glutamate injection after Y-27632 injection into the NTS was

Baseline MAP and HR Values (n=5 for each)

WKY-MAP					
Glu concentration	Control	After Glu	Control	After Y	After Glu
2.0 pmol	101±2	94±2	104±2	98±1	86±1
20 pmol	94±3	81±3	98±2	93±2	70±1
200 pmol	91±2	60±4	100±2	94±1	53±2
WKY-HR					
Glu concentration	Control	After Gill	Control	After Y	After Glu
2.0 pmol	309±7	304±6	304±7	301±6	292±7
20 pmol	301±6	294±6	295±7	291±8	274±10
200 pmol	299±8	276±9	305±7	300±8	269±10
SHR-MAP					
Glu concentration	Control	After Glu	Control	After Y	After Glu
2.0 pmol	163±2	159±2	163±2	146±4*	134±4
20 pmol	161±7	152±7	169±5	150±4†	122±4
200 pmol	167±3	141±4	166±3	151±6*	116±6
SHR-HR					
Glu concentration	Control	After Glu	Control	After Y	After Glu
2.0 pmol	320±4	314±3	325±3	308±6*	299±5
20 pmol	324±7	312±8	315±6	302±4*	279±4
200 pmol	313±4	276±6	317±5	295±7*	249±10

*$P<0.05$; †$P<0.01$ vs control.
Glu indicates glutamate; Y, Y-27632 (40 pmol;0.5 mmol/L in 80 nL).

significantly greater compared with glutamate injection alone in both strains (Figures 2 and 3). However, the magnitude of the augmentation was significantly greater in SHR than in WKY (glutamate dose 2 pmol: 1.8±0.2 versus 4.0±0.3; 20 pmol: 1.7±0.3 versus 3.1±0.3; 200 pmol: 1.2±0.1 versus 1.4±0.2; data are expressed as the relative ratio of the percent change compared with only glutamate injection, which was assigned a value of 1; $P<0.05$; n=5 for each). The magnitude of the HR decrease evoked by unilateral glutamate injection after Y-27632 injection into the NTS was significantly greater compared with only glutamate injection in both strains (Figures 2 and 3). Preinjection of a-CSF did not change the magnitude of the decrease in MAP induced by glutamate injection into the NTS (Figure 4A). The perfusion of NMDA unilaterally into the NTS through a dialysis probe decreased MAP, as reported previously.[18] The magnitude of the decrease in MAP induced by NMDA with Y-27632 injection was significantly greater than that by NMDA perfusion alone (Figure 4B).

Effects of Rho-Kinase Inhibition on Neuronal Activity in the NTS

Twelve neurons responded to iontophoretically applied NMDA and AMPA. Iontophoretic application of NMDA and AMPA transiently increased neuronal activity (Figure 5). Perfusion of Y-27632 increased neuronal activity evoked by NMDA and AMPA (NMDA 1.22±0.19 versus 1.78±0.19 spikes/s; $P<0.05$; AMPA 0.98±0.09 versus 1.33±0.11 spikes/s; n=12 for each; $P<0.05$).

Discussion

The present study demonstrated that inhibition of Rho-kinase activity in the NTS enhances glutamate sensitivity in WKY and SHR, and might improve the impaired glutamate sensitivity in SHR. The present observation might elucidate, at least in part, the mechanisms underlying differences in glutamate sensitivity in the NTS between WKY and SHR reported previously.[23] The glutamate concentration in the NTS is greater in SHR than in WKY.[24] These findings suggest that glutamate sensitivity in the NTS is decreased in SHR compared with WKY.

There is extensive literature regarding glutamate injections into the NTS of SHR and WKY.[25–27] Most of these studies report a similar depressor response to glutamate injected into the NTS between WKY and SHR. We reported a similar result in the previous study.[7] When we examined the dose response to glutamate injections in the present study; how-

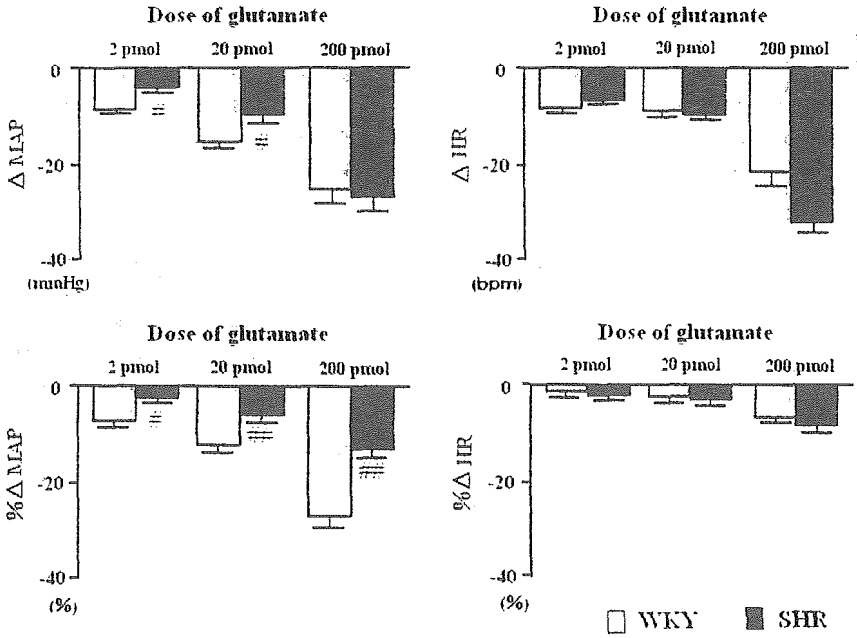

Figure 1. Effect of unilateral microinjection of glutamate into the NTS of WKY and SHR. Grouped data of responses evoked by unilateral injection of glutamate into the NTS (n=8 for each). #$P<0.05$; ##$P<0.01$ vs WKY.

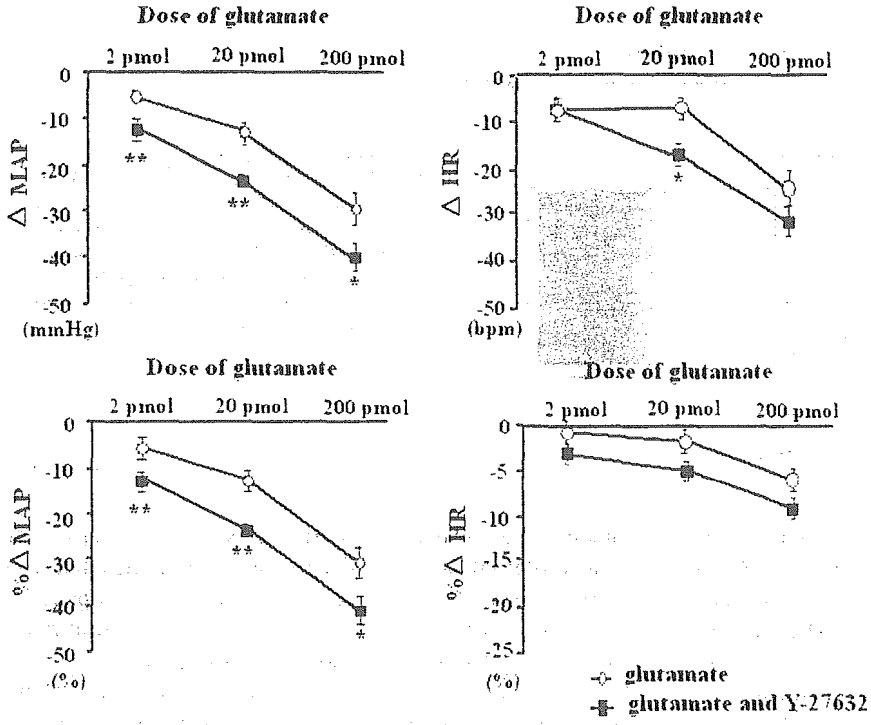

Figure 2. Effect of Rho-kinase inhibition on glutamate sensitivity in the NTS of WKY (n=5 for each). *$P<0.05$; **$P<0.01$ vs injection of only glutamate.

ever, there was less MAP reduction, particularly at lower doses, in SHR than in WKY. This result is consistent with that reported by Talman and Lewis.[23] However, it is difficult to compare the changes in MAP because there are baseline differences between the 2 groups. Talman and Lewis analyzed the data using repeated-measures ANOVA and covariate analysis to address the different MAP baseline values.[23] In the present study, we analyzed the data using a 2-way ANOVA with multiple comparison. Furthermore, we also compare the depressor response by percent change, as used previously.[28] In addition, there are structural vascular changes in SHR than in WKY.[29] Therefore, a greater depressor response is expected in SHR than in WKY. Nonetheless, a depressor response was demonstrated, suggesting an attenuated response to glutamate in SHR.

In the present study, we examined the effects of a Rho-kinase inhibitor on the decrease in arterial pressure evoked by unilateral glutamate injection into the NTS. The decrease in arterial pressure caused by glutamate injection after injection of Y-27632 was significantly greater than that by glutamate injec-

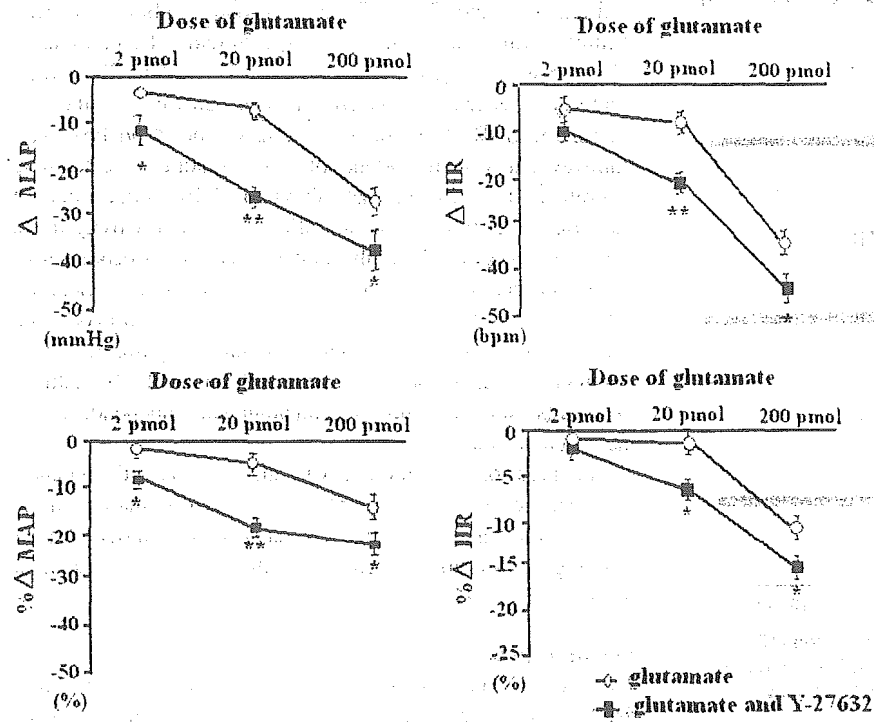

Figure 3. Effect of Rho-kinase inhibition on glutamate sensitivity in the NTS of SHR (n=5 for each). *$P<0.05$; **$P<0.01$ vs injection of only glutamate.

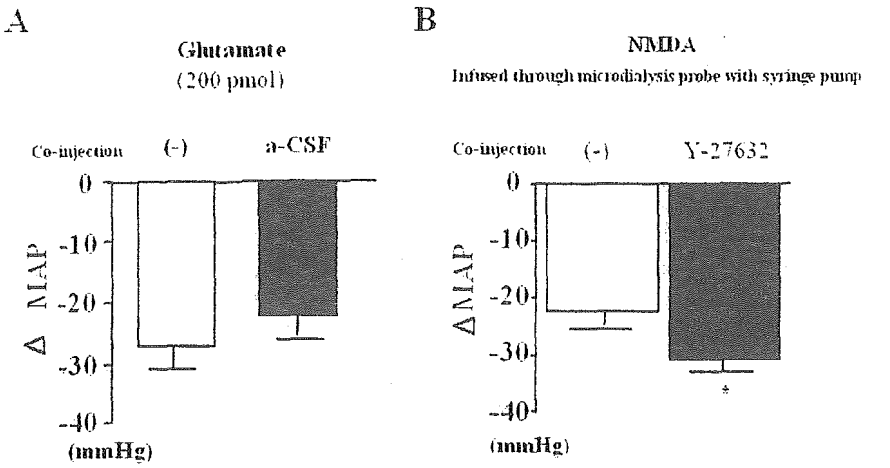

Figure 4. A, Effect of a-CSF on glutamate sensitivity in the NTS of WKY (n=3 for each). B, Effect of Rho-kinase inhibition on NMDA sensitivity in the NTS of WKY. NMDA and Y-27632 were applied using a microdialysis probe with a syringe pump (n=6 for each). *$P<0.05$ vs infusion of only NMDA.

tion alone in both strains. However, the magnitude of the augmentation was significantly greater in SHR than that in WKY, suggesting that inhibition of Rho-kinase in the NTS improves the impaired glutamate sensitivity in SHR. The HR responses to glutamate injection into the NTS did not differ between WKY and SHR (Figure 1), probably because this experiment was performed under anesthesia. However, the magnitude of HR reduction caused by glutamate was significantly augmented by preinjection of Y-27632 (Figures 2 and 3).

We took special care with the microinjection of glutamate to minimize differences in the amount of drug spread. However, differential drug spread is still possible, so we also used a microdialysis probe with an injection line that was connected to a syringe pump. Y-27632 was injected directly through the injection line, and NMDA was infused through the microdialysis probe, as described previously.[18] Infusion of only NMDA into the NTS decreased arterial pressure, as reported previously,[18] and infusion of NMDA with Y-27632 injection also decreased arterial pressure. However, the magnitude of the decrease in arterial pressure was significantly greater after infusion of NMDA with Y-27632 than that with NMDA alone. Therefore, the augmentation of the response to glutamate injection into the NTS is not likely to be attributable to differences in the amount of drug spread.

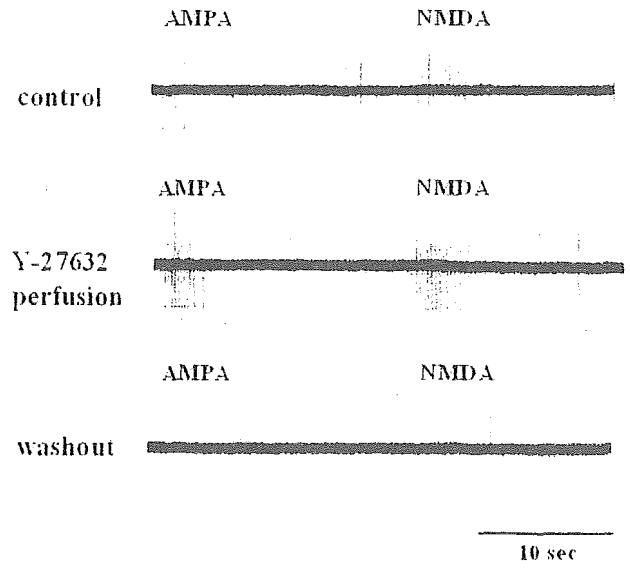

Figure 5. Effects of Y-27632 on neuronal activity in the NTS evoked by iontophoretically applied NMDA or AMPA. Example of raw neurograms indicating the increased neuronal activity after Y-27632 perfusion.

In the microinjection study, the effect of Rho-kinase inhibition on glutamate sensitivity was demonstrated indirectly. Therefore, we then recorded single-unit activity of NTS neurons to examine the direct effects of Rho-kinase inhibition. In the single-unit recording study, Rho-kinase inhibition increased the response of the recorded neurons to NMDA or AMPA. The magnitude of the augmentation differed in each recorded neuron. Because the NTS contains heterogenous neurons, including neurons related to cardiovascular control, it is possible that some of the recorded neurons did not contribute to baroreflex function, which might account for the different effects of Rho-kinase inhibition on the neurons.

We confirmed previously that the Rho/Rho–kinase pathway is activated in the NTS of SHR using Western blot analysis for membranous RhoA (translocation) or the phosphorylated ERM family (ezrin, radixin, moesin; target proteins of Rho-kinase).[7] These results suggest that activation of the Rho/Rho–kinase pathway is related to impaired glutamate sensitivity of the NTS neurons in SHR. As reported previously,[5] the Rho/Rho–kinase pathway plays an important role in regulating vascular tone. Therefore, it is possible that inhibition of Rho-kinase activity increases local blood flow and affects neuronal activity in the NTS. We consider it highly unlikely that the effects of Rho-kinase inhibition on arterial pressure regulation or neuronal activity in the NTS were caused by a local vasodilator effect because microinjection of another vasodilator, hydralazine, does not alter arterial pressure in either WKY or SHR.[7] In addition, the results using the brain slice preparation are independent from the vascular system.

In conclusion, inhibition of Rho-kinase in the NTS enhances glutamate sensitivity in the NTS. The Rho/Rho–kinase pathway in the NTS might be related to mechanism(s) underlying the resetting of baroreflex function in SHR via impaired glutamate sensitivity.

Perspectives

The precise mechanisms by which Rho-kinase inhibition in the NTS increases glutamate sensitivity cannot be elucidated

from the results of the present study. The small GTPase Rho and its downstream effector Rho-kinase are involved in many cellular functions.[30,31] The neuronal Rho/Rho–kinase pathway contributes to dendritic spine formation,[10] which forms the postsynaptic contact site for the majority of excitatory synapses.[11] Morphological changes in dendritic spines occur rapidly[13] and are associated with glutamate sensitivity.[14] Recently, it was demonstrated that there are structural differences in dendritic spines in the NTS between WKY and SHR.[32] However, that study also demonstrated that there were more GluR1-containig dendritic spines in the NTS of SHR compared with WKY, which was attributed to an increase in the proportion of dendritic spines containing GluR1 as well as an increase in the total number of dendritic spines.[32] Thus, it is unlikely that our observations are attributable to the morphological changes resulting from inhibition of the Rho/Rho–kinase pathway. Therefore, the effects of Rho-kinase inhibition might be produced not by the morphological changes in the dendritic spines (ie, an increase in the number of dendritic spines) but rather by a functional change in dendritic spines or other unknown mechanisms. Further studies are needed to clarify the mechanisms underlying our observations.

Acknowledgments

This study was supported by a grant-in-aid for scientific research (C13670721) from Japan Society for the Promotion of Science and by a grant for research on the autonomic nervous system and hypertension from Kimura Memorial Heart Foundation/Pfizer Pharmaceuticals, Inc.

References

1. Matsui T, Amano M, Yamamoto T, Chihara K, Nakafuku M, Ito M, Nakao T, Okawa K, Iwamatsu A, Kaibuchi K. Rho-associated kinase, a novel serine/threonine kinase, as a putative target for the small GTP binding protein Rho. *EMBO J.* 1996;15:2208–2216.
2. Laufs U, Liao JK. Targeting Rho in cardiovascular disease. *Circ Res.* 2000;87:526–528.
3. Kureishi Y, Kobayashi S, Amano M, Kimura K, Kanaide H, Nakano T, Kaibuchi K, Ito M. Rho-associated kinase directly induces smooth muscle contraction through myosin light chain phosphorylation. *J Biol Chem.* 1997;272:12257–12260.
4. Uehata M, Ishizaki T, Satoh H, Ono T, Kawahara T, Morishita, Tamakawa H, Yamagami K, Inui J, Maekawa M, Narumiya S. Calcium sensitization of smooth muscle mediated by a Rho-associated protein kinase in hypertension. *Nature.* 1997;389:990–994.
5. Mukai Y, Shimokawa H, Matoba T, Kandabashi T, Satoh S, Hiroki J, Kaibuchi K, Takeshita A. Involvement of Rho-kinase in hypertensive vascular disease: a novel therapeutic target in hypertension. *FASEB J.* 2001;15:1062–1064.
6. Masumoto A, Hirooka Y, Shimokawa H, Hironaga K, Setoguchi S, Takeshita A. Possible involvement of Rho-kinase in the pathogenesis of hypertension in humans. *Hypertension.* 2001;38:1307–1310.
7. Ito K, Hirooka Y, Sakai K, Kishi T, Kaibuchi K, Shimokawa H, Takeshita A. Rho/Rho-kinase pathway in brain stem contributes to blood pressure regulation via sympathetic nervous system: possible involvement in neural mechanisms of hypertension. *Circ Res.* 2003;92:1337–1343.
8. Ito K, Hirooka Y, Kishi T, Kimura Y, Kaibuchi K, Shimokawa H, Takeshita A. Rho/Rho-kinase pathway in the brainstem contributes to hypertension caused by chronic nitric oxide synthase inhibition. *Hypertension.* 2004;43:156–162.
9. Ito K, Hirooka Y, Sagara Y, Kimura Y, Kaibuchi K, Shimokawa H, Takeshita A, Sunagawa K. Inhibition of Rho-kinase in the brainstem augments baroreflex control of heart rate in rats. *Hypertension.* 2004;44:478–483.
10. Nakayama AY, Harms MB, Luo L. Small GTPases Rac and Rho in the maintenance of dendritic spines and branches in hippocampal pyramidal neurons. *J Neurosci.* 2000;20:5329–5338.
11. Koch C, Zador A. The function of dendritic spines: devices subserving biochemical rather than electrical compartmentalization. *J Neurosci.* 1993;13:413–422.
12. Bito H, Furuyashiki T, Ishihara H, Shibasaki Y, Ohashi K, Mizuno K, Maekawa M, Ishizaki T, Narumiya S. A critical role for a Rho-associated kinase, p160ROCK, in determining axon outgrowth in mammalian CNS neurons. *Neuron.* 2000;26:431–441.
13. Fischer M, Kaech S, Knutti D, Matus A. Rapid actin-based plasticity in dendritic spines. *Neuron.* 1998;20:847–854.
14. Matsuzaki M, Ellis-Davies GC, Nemoto T, Miyashita Y, Iino M, Kasai H. Dendritic spine geometry is critical for AMPA receptor expression in hippocampal CA1 pyramidal neurons. *Nat Neurosci.* 2001;4:1086–1092.
15. Nakazawa T, Watabe AM, Tezuka T, Yoshida Y, Yokoyama K, Umemori H, Inoue A, Okabe S, Manabe T, Yamamoto T. p250GAP, a novel brain-enriched GTPase-activating protein for Rho family GTPases, is involved in the *N*-methyl-D-aspartate receptor signaling. *Mol Biol Cell.* 2003;14:2921–2934.
16. Paxinos G, Watson C. *The Rat Brain in Stereotaxic Coordinates.* 4th ed. New York, NY: Academic Press; 1998.
17. Shigematsu H, Hirooka Y, Eshima K, Shihara M, Tagawa T, Takeshita A. Endogenous angiotensin II in the NTS contributes to sympathetic activation in rats with aortocaval shunt. *Am J Physiol.* 2001;280:R1665–R1673.
18. Matsuo I, Hirooka Y, Hironaga K, Eshima K, Shigematsu H, Shihara M, Sakai K, Takeshita A. Glutamate release via NO production evoked by NMDA in the NTS enhances hypotension and bradycardia in vivo. *Am J Physiol.* 2001;280:R1285–R1291.
19. Shihara M, Hirooka Y, Hori N, Matsuo I, Tagawa T, Suzuki S, Akaike N, Takeshita A. Endothelin-1 increases the neuronal activity and augments the responses to glutamate in the NTS. *Am J Physiol.* 1998;44:R658–R665.
20. Shihara M, Hori N, Hirooka Y, Eshima K, Akaike N, Takeshita A. Cholinergic systems in the nucleus of the solitary tract of rats. *Am J Physiol.* 1999;276:R1141–R1148.
21. Tagawa T, Imaizumi T, Harada S, Endo T, Shiramoto M, Hirooka Y, Takeshita A. Nitric oxide influences neuronal activity in the nucleus tractus solitarius of rat brainstem slices. *Circ Res.* 1994;75:70–76.
22. Hori N, Auker CR, Braitman DJ, Carpenter DO. Pharmacologic sensitivity of amino acid responses and synaptic activation of in vitro prepyriform neurons. *J Neurophysiol.* 1982;48:1289–1301.
23. Talman WT, Lewis SJ. Altered cardiovascular responses to glutamate and acetylcholine microinjected into the nucleus tractus solitarii of the SHR. *Clin Exp Hypertens.* 1991;13:661–668.
24. Kubo T, Kihara M, Misu Y. Altered amino acid levels in brainstem regions of spontaneously hypertensive rats. *Clin Exp Hypertens.* 1996;11:233–241.
25. Katsunuma N, Tsukamoto K, Ito S, Kanmatsuse K. Enhanced angiotensin-mediated responses in the nucleus tractus solitarii of spontaneously hypertensive rats. *Brain Res Bull.* 2003;60:209–214.
26. Matsumura K, Averill DB, Ferrario CM. Angiotensin II acts at AT1 receptors in the nucleus of the solitary tract to attenuate the baroreceptor reflex. *Am J Physiol.* 1998;275:R1611–R1619.
27. Abdel-Rahman AA, Tao S. Differential alteration of neuronal and cardiovascular responses to adenosine microinjected into the nucleus tractus solitarius of spontaneously hypertensive rats. *Hypertension.* 1996;27:939–948.
28. Tsukamoto K, Sved AF, Ito S, Komatsu K, Kanmatsuse K. Enhanced serotonin-mediated responses in the nucleus tractus solitarius of spontaneously hypertensive rats. *Brain Res.* 2000;863:1–8.
29. Folkow B. Physiological aspects of primary hypertension. *Physiol Rev.* 1982;62:347–504.
30. Kimura K, Ito M, Amano M, Chihara K, Fukata Y, Nakafuku M, Yamamori B, Feng J, Nakano T, Okawa K, Iwamatsu A, Kaibuchi K. Regulation of myosin phosphatase by Rho and Rho-associated kinase (Rho-kinase). *Science.* 1996;273:245–248.
31. Kawano Y, Fukata Y, Oshiro N, Amano M, Nakamura T, Ito M, Matsumura F, Inagaki M, Kaibuchi K. Phosphorylation of myosin binding subunit(MBS) of myosin phosphatase by Rho-kinase in vivo. *J Cell Biol.* 1999;147:1023–1037.
32. Aicher SA, Sharma S, Mitchell JL. Structural changes in AMPA-receptive neurons in the nucleus of the solitary tract of spontaneously hypertensive rats. *Hypertension.* 2003;41:1246–1252.

Circulation
JOURNAL OF THE AMERICAN HEART ASSOCIATION

Rho-Kinase Inhibitor Improves Increased Vascular Resistance and Impaired Vasodilation of the Forearm in Patients With Heart Failure

Takuya Kishi, Yoshitaka Hirooka, Akihiro Masumoto, Koji Ito, Yoshikuni Kimura, Kosuke Inokuchi, Tatsuya Tagawa, Hiroaki Shimokawa, Akira Takeshita and Kenji Sunagawa

Circulation 2005;111;2741-2747
DOI: 10.1161/CIRCULATIONAHA.104.510248
Circulation is published by the American Heart Association. 7272 Greenville Avenue, Dallas, TX 72514
 Print ISSN: 0009-7322. Online ISSN: 1524-4539

Rho-Kinase Inhibitor Improves Increased Vascular Resistance and Impaired Vasodilation of the Forearm in Patients With Heart Failure

Takuya Kishi, MD, PhD; Yoshitaka Hirooka, MD, PhD; Akihiro Masumoto, MD, PhD; Koji Ito, MD, PhD; Yoshikuni Kimura, MD; Kosuke Inokuchi, MD; Tatsuya Tagawa, MD, PhD; Hiroaki Shimokawa, MD, PhD; Akira Takeshita, MD, PhD; Kenji Sunagawa, MD, PhD

Background—Rho-kinase is suggested to have an important role in enhanced vasoconstriction in animal models of heart failure (HF). Patients with HF are characterized by increased vasoconstriction and reduced vasodilator responses to reactive hyperemia and exercise. The aim of the present study was to examine whether Rho-kinase is involved in the peripheral circulation abnormalities of HF in humans with the Rho-kinase inhibitor fasudil.

Methods and Results—Studies were performed in patients with HF (HF group, n=26) and an age-matched control group (n=26). Forearm blood flow was measured with a strain-gauge plethysmograph during intra-arterial infusion of graded doses of fasudil or sodium nitroprusside. Resting forearm vascular resistance (FVR) was significantly higher in the HF group than in the control group. The increase in forearm blood flow evoked by fasudil was significantly greater in the HF group than in the control group. The increased FVR was decreased by fasudil in the HF group toward the level of the control group. By contrast, FVR evoked by sodium nitroprusside was comparable between the 2 groups. Fasudil significantly augmented the impaired ischemic vasodilation during reactive hyperemia after arterial occlusion of the forearm in the HF group but not in the control group. Fasudil did not augment the increased FVR evoked by phenylephrine in the control group significantly.

Conclusions—These results indicate that Rho-kinase is involved in increased FVR and impaired vasodilation of the forearm in patients with HF. (*Circulation*. 2005;111:2741-2747.)

Key Words: heart failure ■ blood flow ■ vasoconstriction ■ vasodilation

Increased peripheral vascular resistance and impaired vasodilation of the peripheral vasculature are characteristic in patients with heart failure (HF).[1,2] These characteristics cause fatigue and exercise intolerance in patients with HF and are considered to be mainly due to enhanced sympathetic drive and activation of the renin-angiotensin system.[1–3] The dysfunction of vasodilator factors such as nitric oxide and atrial natriuretic peptide is also involved.[4–10] Ischemia- and exercise-induced vasodilation of the extremities of patients with HF is markedly attenuated, and decreased exercise tolerance in patients with HF is not only due to impaired pump function of the heart but also to inadequate increases in muscle blood flow as a result of impaired vasodilation during exercise.[2,5] Increased peripheral resistance and impaired vasodilation are consistent findings in HF.[1,2,5–8] The molecular mechanisms underlying impaired vasodilation in patients with HF, however, remain to be elucidated.

Myosin light chain (MLC) phosphorylation is a crucial step for vascular smooth muscle cell (VSMC) contraction, which is regulated in a dual manner by MLC kinase and MLC phosphatase.[11] Inhibition of MLC phosphatase results in increased MLC phosphorylation and subsequent VSMC hypercontraction (Ca^{2+} sensitization).[11,12] This mechanism of Ca^{2+} sensitization in VSMCs is enhanced in animal models of HF.[13] Rho-kinase/ROKα/RockII, which is activated by the small GTPase Rho, inhibits MLC phosphatase activity and thus plays a key role in Ca^{2+} sensitization and hypercontraction of VSMCs.[11,12,14] Y-27632, a Rho-kinase inhibitor, preferentially lowers arterial pressure in rat models of hypertension in vivo, which indirectly suggests an involvement of Rho-kinase in hypertension.[15] We recently demonstrated that Rho-kinase is upregulated and plays a key role in VSMC contraction in a porcine model of coronary artery spasm[16,17] and in spontaneously hypertensive rats[18] and that Rho-kinase might be involved in the pathogenesis of increased peripheral vascular resistance in hypertension in humans.[19] Previous reports suggest that the Rho/Rho-kinase pathway plays a critical role in Dahl salt-sensitive hypertensive rats with congestive HF[20] and might be involved in the enhanced arterial vasoconstriction in tachycardia-induced HF in dogs.[13]

Received September 30, 2004; revision received January 20, 2005; accepted February 23, 2005.

From the Department of Cardiovascular Medicine, Kyushu University Graduate School of Medical Sciences, Fukuoka, Japan.

Correspondence to Yoshitaka Hirooka, MD, PhD, FAHA, Department of Cardiovascular Medicine, Kyushu University Graduate School of Medical Sciences, 3-1-1 Maidashi, Higashi-ku, Fukuoka 812-8582, Japan. E-mail hyoshi@cardiol.med.kyushu-u.ac.jp

Circulation is available at http://www.circulationaha.org

DOI: 10.1161/CIRCULATIONAHA.104.510248

It is unknown, however, whether this is also the case in human patients with HF.

The present study was designed to determine whether Rho-kinase is involved in the increased peripheral vascular resistance in patients with HF by examining the vasodilator effect of a specific Rho-kinase inhibitor, fasudil. Fasudil is currently used in Japan for the treatment of cerebral vasospasm after subarachnoid hemorrhage.[21] Fasudil is a specific Rho-kinase inhibitor, as is Y-27632,[15,16,22,23] although the latter is not yet approved for human use. We recently used fasudil to examine forearm vascular resistance in patients with hypertension, and there were no complications.[19] Thus, fasudil is regarded as a specific Rho-kinase inhibitor that can be used safely in humans.

Methods

Patients

Twenty-six patients with HF (HF group; 17 men, 9 women; mean age 63±3 years) and 26 control subjects (control group; 15 men, 11 women; mean age 60±6 years) were enrolled in the present study. The HF group comprised 17 patients with ischemic heart disease, 8 patients with dilated cardiomyopathy, and 1 patient with valvular heart disease. All patients with HF were diagnosed according to the Framingham criteria.[24] Physical activity was determined on the basis of the New York Heart Association (NYHA) functional class. There were 14 patients with NYHA class 3 and 12 patients with NYHA class 2 in the HF group. Systemic hypertension was defined as systolic blood pressure >140 mm Hg or diastolic blood pressure >90 mm Hg. Hyperlipidemia was defined as serum total cholesterol >220 mg/dL or serum triglyceride levels >150 mg/dL. Diabetes mellitus was defined as fasting blood sugar >110 mg/dL. Left ventricular ejection fraction was determined by the modified Simpson method or single-plane area-length method on echocardiogram. We defined the control group as a non-HF/nonhypertensive group. Subjects in the control group were admitted to our hospital because of atypical chest pain, fatigue, or palpitations. Careful examination was performed to rule out coronary artery disease (by coronary angiography) and other organic heart diseases (echocardiogram) or arrhythmia (Holter ECG or ECG monitoring during hospitalization and/or electrophysiological study). In the control group, 5 subjects had serum total cholesterol levels >220 mg/dL, and 4 had serum triglyceride levels >150 mg/dL. Serum total cholesterol levels were <250 mg/dL, and serum triglyceride levels were <180 mg/dL, even in the HF group. Six subjects had a history of smoking; however, they had quit smoking before admission. This was also true in the HF group. Some subjects in the control group transiently received some medications, such as ACE inhibitors, an angiotensin II (Ang II) receptor blocker, or a β-blocker, from general practitioners because of mild high blood pressure and/or palpitations after our careful interviews. The subjects, however, did not take those medications continuously, and we confirmed that they did not have HF, hypertension, or arrhythmias on admission. In contrast, patients in the HF group were given those medications because of HF. It was ethically difficult to discontinue those medications for the purpose of the study. Therefore, the medications were discontinued only on the day of the study, and restarted just after the study. The present study was approved by the ethics committee for human research in our institute, and written informed consent was obtained from each subject.

General Procedures

The present study was performed with subjects in a supine position and in a postabsorptive state with the room temperature at 25°C to 27°C. All medications were withheld on the day of the study. With the subjects under local anesthesia, the left brachial artery was cannulated with a 20-gauge intravascular cannula for drug infusion, and the cannula was connected to a pressure transducer for direct measurement of arterial pressure. The antecubital vein was cannulated, and blood samples were obtained for measurements of serum or plasma chemistry, including plasma brain natriuretic peptide (BNP), Ang II, and norepinephrine (NE).

Measurement of Forearm Blood Flow

Forearm blood flow (FBF) was measured with a strain-gauge plethysmograph with the venous-occlusion technique, as reported previously.[5,19,25–29] FBF (mL · min^{-1} · 100 mL^{-1} of forearm volume) was calculated from the rate of increase in forearm volume while venous return from the forearm was prevented by inflation of a cuff on the upper arm. The pressure in the venous-occlusion or congesting cuff was 40 mm Hg. Circulation to the hand was arrested by inflation of a cuff around the wrist. An average of 4 measurements made at 15-second intervals was used for later analysis. Forearm vascular resistance (FVR) was calculated by dividing mean arterial pressure (diastolic pressure plus one third of pulse pressure in mm Hg) by FBF. FVR was expressed as units.

Study Protocol 1: Effect of Fasudil on FBF and FVR in Patients With HF and in Control Subjects

FBF, arterial pressure, and heart rate were measured at rest and during administration of graded doses of fasudil (3.2, 6.4, 12.8, and 25.6 μg/min) or sodium nitroprusside (SNP; 0.4, 0.8, 1.6, and 3.2 μg/min).[19] Each dose of fasudil was infused for 15 minutes, and FBF was measured during the last minute of each infusion. Each dose of SNP was infused for 5 minutes, and FBF was measured after each infusion. Venous blood samples were drawn from the antecubital vein before and immediately after infusion of the peak dose of fasudil (25.6 μg/min) and at the end of the study for determination of the plasma fasudil concentration.

Study Protocol 2: Effects of Fasudil on FBF and FVR Responses to Reactive Hyperemia in Patients With HF and Control Subjects

We studied 8 patients with HF and 9 control subjects. FBF and FVR were measured as described in study protocol 1. To induce reactive hyperemia, FBF was occluded by inflation of a cuff placed over the left upper arm to a pressure of 200 mm Hg for 5 minutes. After the ischemic cuff occlusion was released, FBF was measured every 15 seconds for 3 minutes. Ten minutes after FBF returned to baseline values, fasudil (25.6 μg/min) was infused for 15 minutes, and the FBF responses to reactive hyperemia were measured by the same procedures described above.

Study Protocol 3: Effects of Fasudil on FBF and FVR During Infusion of Phenylephrine in Control Subjects

To exclude the possibility that baseline differences in FBF might affect the results, we examined the FBF responses evoked by fasudil before and after infusion of phenylephrine (400 ng/min) in control subjects (n=5). FBF, arterial pressure, and heart rate were measured at rest and during administration of graded doses of fasudil (3.2, 6.4, 12.8, and 25.6 μg/min) or SNP (0.4, 0.8, 1.6, and 3.2 μg/min) as described in study protocol 1.

Drugs

The following drugs were used: fasudil hydrochloride hydrate (Eril; Asahi Kasei Pharmaceutical Corporation), SNP (Nitpro Inj; Maruishi Pharmaceutical Co), and phenylephrine hydrochloride (Neosynesin; Kowa Company, Ltd). All drugs were dissolved in physiological saline immediately before use.

Statistical Analysis

All results are expressed as mean±SEM. Values at rest were compared by unpaired t test. Responses to graded doses of drugs in each group were examined by ANOVA for repeated measures. Two-way ANOVA was used to compare FBF, FVR, and reactive hyperemia responses in the 2 groups. The relationship between

Clinical Profiles and Baseline Characteristics of HF Group and Control Group

	HF Group (n=26)	Control Group (n=26)
Age, y	63±3	60±6
Male/female, n	17/9	15/11
BMI, kg/m^2	24±3	25±2
HT/DM/HL, n	0/0/12	0/0/9
LVEF, %	37±4*	62±3
BNP, pg/mL	364±120*	30±13
Ang II, pg/mL	39±6*	18±6
NE, pg/mL	492±193*	190±84
Total cholesterol, mg/dL	208±33	190±29
LDL cholesterol, mg/dL	142±14	130±22
FBS, mg/dL	98±15	89±14
MBP, mm Hg	85±13	86±14
HR, bpm	89±6*	68±8
FBF, mL · min^{-1} · 100 mL^{-1}	3.8±0.4*	5.2±0.6
FVR, U	39±11*	20±4
Fasudil, nmol/L	560±60	526±86

n indicates number of patients or subjects; BMI, body mass index; HT, hypertension; DM, diabetes mellitus; HL, hyperlipidemia; LVEF, left ventricular ejection fraction; FBS, fasting blood sugar; MBP, mean blood pressure; and HR, heart rate.

Data are presented as mean±SEM.

*P<0.05 vs control group.

plasma BNP or Ang II and FBF or FVR on the maximum dose of fasudil was examined with a linear regression analysis with Pearson correlation coefficients. A P value of <0.05 was considered to be statistically significant.

Results

Baseline Characteristics

There was no significant difference in mean blood pressure at rest between the HF and control group (Table). Resting heart rate was significantly higher in the HF group than in the control group (89±6 versus 68±8 bpm, P<0.01; Table). Basal FBF was significantly lower in the HF group than in the control group (3.8±0.4 versus 5.2±0.6 mL · 100 mL^{-1} · min^{-1}, P<0.05; Table). Basal FVR was significantly higher in the HF group than in the control group (39±11 versus 20±4 U, P<0.05; Table). The 2 groups were comparable in age, gender, body mass index, serum total cholesterol, triglycerides, LDL cholesterol, HDL cholesterol, fasting blood sugar, and previous smoking habit (Table). Compared with the control group, the average left ventricular ejection fraction was significantly lower and the average plasma BNP level and plasma concentrations of Ang II and NE were significantly higher in the HF group (Table).

Plasma Concentrations of Fasudil

Just after the peak dose of fasudil, plasma fasudil concentrations significantly increased in both groups; the levels were comparable between groups (560±60 versus 526±86 nmol/L, respectively; Table).

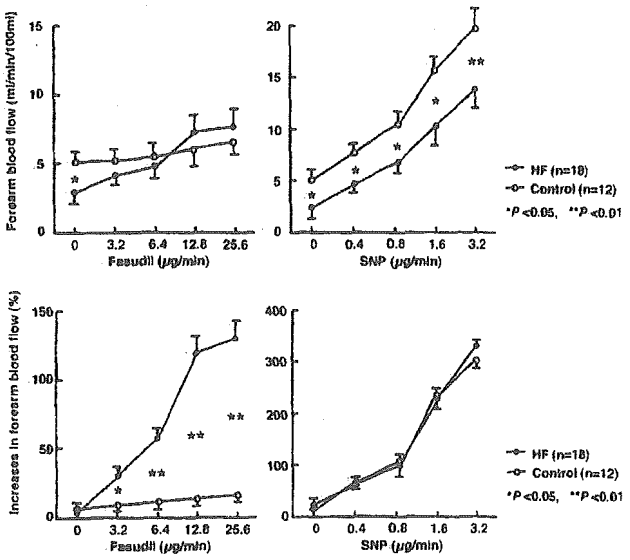

Figure 1. Plots showing responses of FBF to fasudil and SNP as expressed in absolute values (top) and percent change (bottom) in HF group and control group. Results are expressed as mean±SEM.

Forearm Vascular Responses to Fasudil and SNP

Fasudil evoked significant dose-dependent increases in FBF in the HF group but not in the control group (Figure 1). The increase in both the absolute FBF and percent change were apparent only in the HF group (Figure 1). In contrast, SNP induced comparable increases in FBF in the 2 groups (Figure 1). Fasudil evoked significantly greater decreases in both the absolute FVR value and percent change in the HF group compared with the control group, thus normalizing FVR in those patients (Figure 2). In contrast, SNP induced comparable decreases in FVR in both groups (Figure 2). Systemic arterial blood pressure and heart rate did not change signifi-

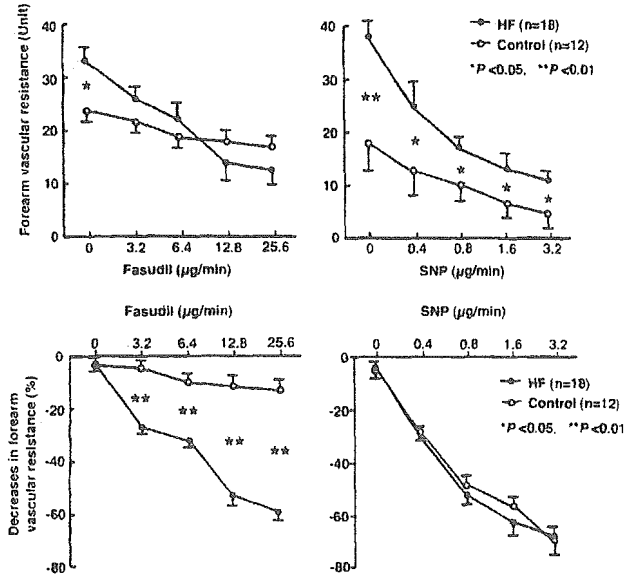

Figure 2. Plots showing responses of FVR to fasudil and SNP as expressed in absolute values (top) and percent change (bottom) in HF group and control group. Results are expressed as mean±SEM.

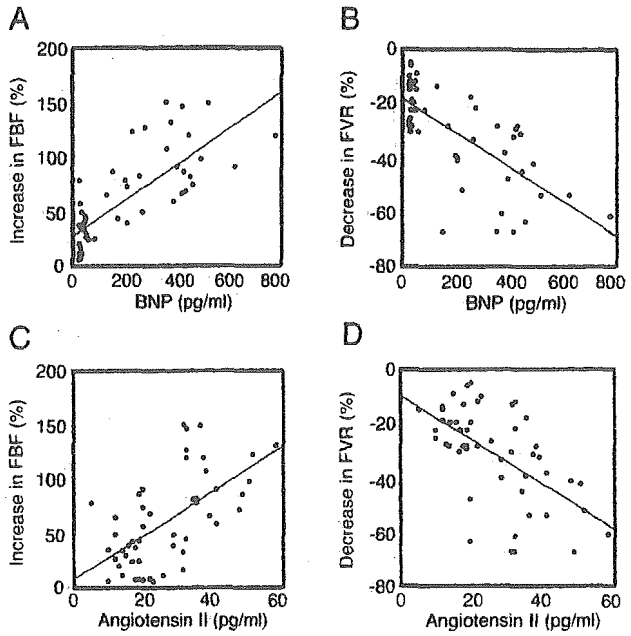

Figure 3. Relation between plasma levels of BNP and increase in FBF (A), plasma levels of BNP and decrease in FVR (B), plasma levels of Ang II and increase in FBF (C), and plasma levels of Ang II and decrease in FVR (D).

cantly during intra-arterial infusion of fasudil or SNP in either group. With the maximum dose of fasudil, there was a significant positive correlation between BNP and the increase in FBF ($r=0.6$, $P=0.002$; Figure 3A), and there was a significant negative correlation between BNP and the decrease in FVR ($r=-0.45$, $P=0.006$; Figure 3B). Moreover, with the maximum dose of fasudil, there was a significant positive correlation between plasma levels of Ang II and the increase in FBF ($r=0.54$, $P=0.001$; Figure 3C), and there was a significant negative correlation between plasma levels of Ang II and the decrease in FVR ($r=-0.58$, $P=0.005$; Figure 3D). There was, however, no significant correlation between baseline FBF and maximal forearm vasodilation in HF patients ($r=0.15$, $P=0.548$).

Effects of Fasudil on Response of FBF to Reactive Hyperemia

In the HF group, the response to reactive hyperemia was significantly lower than in the control group before the infusion of fasudil. After the infusion of fasudil, in the HF group, the response to reactive hyperemia was augmented to the levels of the control group (Figures 4A and 4C). In the control group, fasudil did not change the response to reactive hyperemia (Figures 4B and 4D).

Effects of Fasudil on FBF and FVR During Infusion of Phenylephrine in Control Group

Phenylephrine (400 ng/min) decreased FBF and increased FVR in the control group to levels comparable to those of the HF group. Fasudil did not significantly change FBF and FVR in the control subjects before or after infusion of phenylephrine (Figure 5). SNP induced comparable increases in FBF and decreases in FVR before and after infusion of phenylephrine (Figure 5).

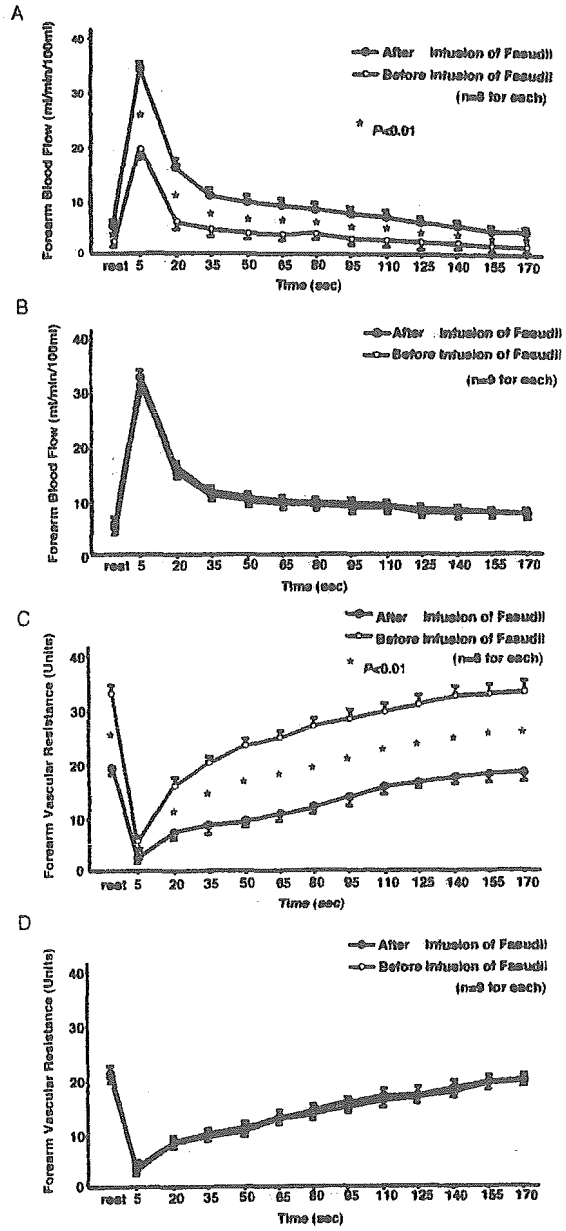

Figure 4. FBF at rest and during reactive hyperemia in HF group (A) and in control group (B) before and after infusion of fasudil. FVR at rest and during reactive hyperemia in HF group (C) and control group (D) before and after infusion of fasudil. Results are expressed as mean±SEM. Probability value refers to comparison of time-course curves with ANOVA for repeated measurements.

Discussion

The major findings of the present study were that (1) the forearm vasodilator response to fasudil was significantly greater in the HF group than in the control group, whereas SNP induced a similar forearm vasodilator response in the 2 groups, and (2) fasudil augmented the impaired response to reactive hyperemia in the HF group. In a similar hypercontractile condition evoked by phenylephrine in the control group, fasudil did not induce the vasodilator response. These results suggest that activation of Rho-kinase is involved in the increased peripheral vascular resistance in patients with HF.

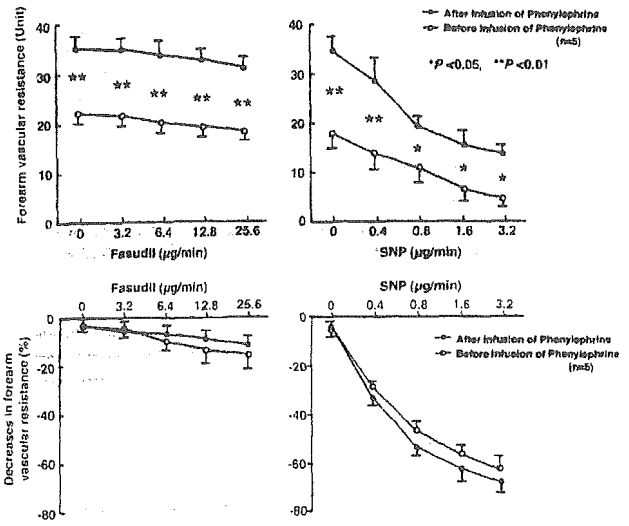

Figure 5. Plots showing responses of FVR in response to fasudil and SNP during infusion of phenylephrine or saline in control group as expressed in absolute values (top) and percent change (bottom). Results are expressed as mean±SEM.

In the present study, basal FVR was significantly higher in the HF group than in the control group, and administration of fasudil into the forearm improved vasodilation and decreased FVR to the levels of the control group. These results suggest that activation of the Rho/Rho-kinase pathway is involved in the hyperconstriction of peripheral arteries in patients with HF. The preferential vasodilator effect of fasudil in the HF group was not due to structural changes in the arterial wall, because the response to SNP was comparable between the 2 groups. Previously, we demonstrated that SNP-induced vasodilation was similar between patients with HF and normal subjects,[5,29] and the response to SNP in the present study was comparable. In the control group, the Rho/Rho-kinase pathway was not significantly activated, because fasudil did not significantly change FBF or FVR. These results are consistent with our previous report.[19] Furthermore, after infusion of phenylephrine in the control group, which decreased FBF to levels similar to those in patients with HF, fasudil did not significantly change FBF and FVR. Thus, the difference in basal FBF does not account for our observation. We cannot exclude the possibility, however, that long-term adrenergic stimulation activates the Rho/Rho-kinase pathway, because NE might activate Rho-kinase.[30] Together with the results of the effects of SNP, these findings suggest that the vasodilator effect of fasudil in the HF group was not due to the structural changes of the arterial wall and that Rho-kinase is involved in the pathogenesis of increased peripheral vascular resistance in patients with HF. Furthermore, we consider that the vascular effects of fasudil are independent of the basal FBF.

Previous studies suggested that maximal vasodilation is impaired in patients with HF.[1,2,5–8] The findings of the present study are consistent with this suggestion. In the present study, submaximal vasodilation induced by ischemia (reactive hyperemia) was significantly impaired in the HF group, and fasudil increased the maximal FBF and decreased the minimal FVR. These responses were not observed in the control group. We evaluated forearm vasodilating responses induced by reactive hyperemia during infusion of the maximum dose of fasudil, which increased FBF and decreased FVR in the HF group, by examining the effect of fasudil-induced Rho-kinase inhibition. At this dose of fasudil, baseline FBF and FVR were comparable between the 2 groups (Figure 4). These results indicate that activation of the Rho/Rho-kinase pathway is involved in impaired vasodilation induced by metabolic stimulation in patients with HF.

In the present study, the plasma concentrations of fasudil were not significantly different between the 2 groups. We and others previously demonstrated that the IC_{50} value of fasudil is <1.9 μmol/L when tested in vitro,[16,22] and the achieved concentration in patients in the present study was high enough to inhibit Rho-kinase activity. We previously demonstrated that fasudil augmented the impaired vasodilation in patients with hypertension,[19] and we used the same dose in the present study. Fasudil prevents acetylcholine-induced coronary artery spasm and the resultant myocardial ischemia in patients with vasospastic angina[31] and coronary microvascular spasm.[32] Noma et al[33] demonstrated that smoking activates Rho-kinase in forearm VSMCs but does not alter the vasodilating effect induced by exogenous nitric oxide in forearm VSMCs in healthy young men. In that study, graded doses of fasudil (3, 10, and 30 μg/min) were infused for 5 minutes, but the plasma fasudil concentration was not measured. We used a similar dose of fasudil administered for a longer period of time. These results suggest that the dose of fasudil selectively and specifically inhibited Rho-kinase.

Vasodilation evoked by fasudil correlated to the plasma BNP levels, which suggests that activation of the Rho/Rho-kinase pathway is related to the severity of HF.[34] Plasma BNP levels are now widely accepted as a prognostic marker of HF. In contrast, the basic disorder of HF did not correlate to the extent of vasodilation evoked by fasudil, which suggests that activation of the Rho/Rho-kinase pathway in the forearm vasculature is associated with an HF state rather than basic disorders.

In the present study, 6 control subjects had a "previous" smoking habit. Chronic smoking activates Rho-kinase in forearm VSMCs in healthy young men.[33] In the present study, there was no vasodilator response to fasudil in the control group, even in previous smokers. There was also no significant difference in the responses of FBF and FVR to fasudil between nonsmokers and the previous smokers in the HF and control groups. From these results, we consider that the previous smoking habit had no effects on activation of Rho-kinase in these patients.

Previous studies suggest that hypercholesterolemia impairs endothelial function.[35,36] Creager et al[35] reported that in humans with hypercholesterolemia, whose average serum cholesterol was 275 mg/dL, there is a decreased effect of nitrovasodilators, including endothelium-derived relaxing factor, on the vascular smooth muscle of resistance vessels. Casino et al[36] reported that hypercholesterolemic patients, whose average serum cholesterol levels were 292 mg/dL, have impaired endothelium-dependent vascular relaxation. In the present study, in the control group, 5 subjects had serum total cholesterol levels >220 mg/dL, and 4 had serum triglyceride levels >150 mg/dL. Serum total cholesterol

levels were <250 mg/dL and serum triglyceride levels were <180 mg/dL, however, even in the HF group. Therefore, we consider that these levels of hypercholesterolemia are not enough to activate Rho-kinase.

The present study did not address the precise mechanism(s) by which the Rho/Rho-kinase pathway is activated in patients with HF. In the animal models of HF, however, the Rho/Rho-kinase pathway is reported to be involved in the pathogenesis of HF.[13,20,37] Rho-kinase is substantially involved in the pathogenesis of left ventricular remodeling after myocardial infarction associated with upregulation of proinflammatory cytokines.[37] Differential activation of the Rho/Rho-kinase pathway plays a critical role in HF, and the Rho/Rho-kinase pathway is involved in the pathogenesis of cardiac dysfunction and cardiovascular remodeling.[20] Hisaoka et al[13] demonstrated that the Rho/Rho-kinase system is critically involved in the enhanced arterial vasoconstriction observed in HF. In that study, enhanced vasoconstriction was induced by a marked increase in Ca^{2+} sensitivity mediated through activation of the Rho/Rho-kinase pathway.[13] Activation of the sympathetic nervous system and renin-angiotensin system occurs in HF, and this neurohumoral activation causes HF to deteriorate.[2,38] This mechanism is also related to abnormal peripheral circulation in HF.[2,3,39] Previous in vitro studies suggest that Rho-kinase is deeply involved in the Ang II–induced signaling pathway.[40–42] Therefore, those studies suggest that activation of the renin-angiotensin system is upstream of the Rho/Rho-kinase pathway and that Ang II upregulates the Rho-kinase pathway in patients with HF. In fact, several neurohumoral factors such as Ang II, NE, and endothelin-1, which activate the Rho/Rho-kinase pathway, are increased in patients with HF.[39,43] In the present study, we evaluated the correlation between plasma Ang II levels and the increases in FBF or the decreases in FVR caused by the infusion of fasudil. These results suggest that there is a correlation between plasma Ang II levels and Rho-kinase activity.

Furthermore, fasudil likely influences endothelial function. In fact, recent studies suggest an interaction between endothelial NO synthase activity and Rho-kinase.[44] For example, it is suggested that NO induces vasodilation through inhibition of the Rho/Rho-kinase signaling pathway and that the Rho/Rho-kinase activity negatively regulates endothelial NO synthase phosphorylation.[45] It is well established that NO activity is decreased in HF.[6–10] In addition, we previously demonstrated that L-arginine supplementation improves both acetylcholine-induced and reactive hyperemia–induced forearm vasodilation in patients with HF, which suggests that the impaired vasodilation is caused by reduced NO activity in HF.[5] Therefore, it is possible that inhibition of Rho-kinase improves NO activity in patients with HF. We did not address this issue in the present study. We do consider, however, that inhibition of Rho-kinase has multiple actions, including modulation of both endothelial and VSMC function. Because Rho-kinase causes VSMC hypercontraction via a Ca^{2+}-sensitizing mechanism, it is difficult to exclude the possibility that fasudil acts directly on VSMCs. Also, in an in vitro study, activation of the Rho/Rho-kinase pathway was involved in arterial hypercontraction in an HF model through a Ca^{2+}-sensitization mechanism.[13] Thus, we suggest that abnormalities of both endothelial and VSMC function are involved in the effects of fasudil on the increased vascular resistance in patients with HF. Further studies are needed to examine this issue.

In conclusion, the present study indicates that fasudil, a Rho-kinase inhibitor, improves the increased FVR and impaired vascular response to reactive hyperemia in the forearm of patients with HF and that these effects are not due to changes in the vascular structures.

Clinical Implications

We demonstrated that the Rho/Rho-kinase pathway is involved in the pathogenesis of HF. Thus, inhibition of the Rho-kinase pathway might be a potential therapeutic strategy for HF. Our results suggest that inhibition of Rho-kinase might improve abnormal peripheral circulation, thereby augmenting exercise tolerance in patients with HF.[2,3,39] Furthermore, Rho-kinase is substantially involved in the pathogenesis of left ventricular remodeling after myocardial infarction associated with upregulation of proinflammatory cytokines,[37] which suggests that these molecular mechanisms might be important targets for the prevention of post–myocardial infarction HF.

Acknowledgments

This study was supported by grants-in-aid from the Japan Society for the Promotion of Science (C13670721 and C15590757) and by grants for the study of clinical vascular function from the Kimura Memorial Heart Foundation.

References

1. Zelis R, Mason DT, Braunwald E. A comparison of the effects of vasodilator stimuli on peripheral resistance vessels in normal subjects and in patients with congestive heart failure. *J Clin Invest*. 1968;47:960–970.
2. Zelis R, Flaim SF. Alterations in vasomotor tone in congestive heart failure. *Prog Cardiovasc Dis*. 1982;24:437–459.
3. Grassi G, Giannattasio C, Failla M, Pesenti A, Marinosi E, Fraschini N, Vailati S, Mancia G. Sympathetic modulation of radial artery compliance in congestive heart failure. *Hypertension*. 1995;26:348–354.
4. Hirooka Y, Takeshita A, Imaizumi T, Suzuki S, Yoshida M, Ando S, Nakamura M. Attenuated forearm vasodilative response to intra-arterial atrial natriuretic peptide in patients with heart failure. *Circulation*. 1990;82:147–153.
5. Hirooka Y, Imaizumi T, Tagawa T, Shiramoto M, Endo T, Ando S, Takeshita A. Effects of L-arginine on impaired acetylcholine-induced and ischemic vasodilation of the forearm in patients with heart failure. *Circulation*. 1994;90:658–668.
6. Drexler H, Hayoz D, Munzel T, Hornig B, Just H, Brunner HR, Zelis R. Endothelial function in chronic congestive heart failure. *Am J Cardiol*. 1992;69:1596–1601.
7. Hambrecht R, Fiehn E, Weigl C, Gielen S, Hamann C, Kaiser R, Yu J, Adams V, Niebauer J, Schuler G. Regular physical exercise corrects endothelial dysfunction and improves exercise capacity in patients with chronic heart failure. *Circulation*. 1998;98:2709–2715.
8. Hornig B, Maier V, Drexler H. Physical training improves endothelial function in patients with chronic heart failure. *Circulation*. 1996;93:210–214.
9. Katz SD, Schwarz M, Yuen J, LeJemtel TH. Impaired acetylcholine-mediated vasodilation in patients with congestive heart failure. *Circulation*. 1993;88:55–61.
10. Kubo SH, Rector TS, Bank AJ, Williams RE, Heifets SM. Endothelium-dependent vasodilation in attenuated in patients with heart failure. *Circulation*. 1991;84:1589–1596.
11. Somlyo AP, Somlyo AV. Signal transduction by G-proteins, rho-kinase and phosphatase to smooth muscle and non-muscle and myosin II. *J Physiol*. 2000;522:177–185.

12. Satoh S, Kreutz R, Wilms C. Augmented agonist-induced Ca^{2+}-sensitization of coronary contraction in genetically hypertensive rats: evidence for altered signal transduction in the coronary smooth muscle cells. *J Clin Invest*. 1997;94:1397–1403.
13. Hisaoka T, Yano M, Ohkusa T, Suetsugu M, Ono K, Kohno M, Yamada J, Kobayashi S, Kohno M, Matsuzaki M. Enhancement of Rho/Rho-kinase system in regulation of vascular smooth muscle contraction in tachycardia-induced heart failure. *Cardiovasc Res*. 2001;49:319–329.
14. Kaibuchi K, Kuroda S, Amano M. Regulation of cytoskeletons and cell adhesions by the Rho family GTPase in mammalian cells. *Annu Rev Biochem*. 1999;68:459–486.
15. Uehata M, Ishizaki T, Satoh H, Ono H, Kawahara T, Morishita T, Tamakawa H, Yamagami K, Inui J, Maekawa M, Narumiya S. Calcium sensitization of smooth muscle mediated by a Rho-associated protein kinase in hypertension. *Nature*. 1997;389:990–994.
16. Shimokawa H, Seto M, Katsumata N, Amano M, Kozai T, Yamawaki T, Kuwata K, Kandabashi T, Egashira K, Ikegami I, Asano T, Kaibuchi K, Takeshita A. Rho-kinase–mediated pathway induces enhanced myosin light chain phosphorylations in a swine model of coronary artery spasm. *Cardiovasc Res*. 1999;43:1029–1039.
17. Kandabashi T, Shimokawa H, Miyata K, Kunihiro I, Kawano Y, Fukata Y, Higo T, Egashira K, Takahashi S, Kaibuchi K, Takeshita A. Inhibition of myosin phosphatase by up-regulated Rho-kinase plays a key role for coronary artery spasm in a porcine model with interleukin-1β. *Circulation*. 2000;101:1319–1323.
18. Mukai Y, Shimokawa H, Matoba T, Kandabashi T, Satoh S, Hiroki J, Kaibuchi K, Takeshita A. Involvement of Rho-kinase in hypertensive vascular disease: a novel therapeutic target in hypertension. *FASEB J*. 2001;15:1062–1064.
19. Masumoto A, Hirooka Y, Shimokawa H, Hironaga K, Setoguchi S, Takeshita A. Possible involvement of Rho-kinase in the pathogenesis of hypertension in humans [published erratum appears in *Hypertension*. 2002:e19]. *Hypertension*. 2001;38:1307–1310.
20. Kobayashi N, Horinka S, Mita S, Nakano S, Honda T, Yoshida K, Kobayashi T, Matsuoka H. Critical role of Rho-kinase pathway for cardiac performance and remodeling in failing rat hearts. *Cardiovasc Res*. 2002;55:757–767.
21. Asano Tm Suzuki M, Tsuchiya S, Satoh S, Ikegaki I, Shibuya M, Suzuki Y, Hidaka H. Vasodilator actions of HA1077 in vitro and in vivo putatively mediated by the inhibition of protein kinase. *Br J Pharmacol*. 1989;98:1091–1100.
22. Davies SP, Reddy H, Caivano M, Cohen P. Specificity and mechanism of action of some commonly used protein kinase inhibitors. *Biochem J*. 2000;351:95–105.
23. Nagumo H, Sasaki Y, Ono Y, Okamoto H, Seto M, Takuwa Y. Rho kinase inhibitor HA-1077 prevents Rho-mediated myosin phosphatase inhibition in smooth muscle cells. *Am J Physiol Cell Physiol*. 2000;278:C57–C65.
24. Mckee PA, Castelli WP, McNamara PM, Kannel WB. The natural history of congestive heart failure: the Framingham study. *N Engl J Med*. 1971;285:1441–1446.
25. Hirooka Y, Imaizumi T, Masaki H, Ando S, Harada S, Momohara M, Takeshita A. Captopril improves impaired endothelium-dependent vasodilation in hypertensive patients. *Hypertension*. 1992;20:175–180.
26. Inokuchi K, Hirooka Y, Shimokawa H, Sakai K, Kishi T, Ito K, Kimura Y, Takeshita A. Role of endothelium-derived hyperpolarizing factor in human forearm circulation. *Hypertension*. 2003;42:919–924.
27. Hirooka Y, Eshima K, Setoguchi S, Kishi T, Egashira K, Takeshita A. Vitamin C improves attenuated angiotensin II–induced endothelium-dependent vasodilation in human forearm vessels. *Hypertens Res*. 2003;26:953–959.
28. Tagawa T, Imaizumi T, Endo T, Shiramoto M, Harasawa Y, Takeshita A. Role of nitric oxide in reactive hyperemia in human forearm vessels. *Circulation*. 1994;90:2285–2290.
29. Setoguchi S, Hirooka Y, Eshima K, Shimokawa H, Takeshita A. Tetrahydrobiopterin improves impaired endothelium-dependent forearm vasodilation in patients with heart failure. *J Cardiovasc Pharmacol*. 2002;39:363–368.
30. Shimokawa H. Rho-kinase as a novel therapeutic target in treatment of cardiovascular diseases. *J Cardiovasc Pharmacol*. 2002;39:319–327.
31. Masumoto A, Mohri M, Shimokawa H, Urakami L, Usui M, Takeshita A. Suppression of coronary artery spasm by the Rho-kinase inhibitor fasudil in patients with vasospastic angina. *Circulation*. 2002;105:1545–1547.
32. Mohri M, Shimokawa H, Hirakawa Y, Masumoto A, Takeshita A. Rho-kinase inhibition with intracoronary fasudil prevents myocardial ischemia in patients with coronary microvascular spasm. *J Am Coll Cardiol*. 2003;41:15–19.
33. Noma K, Higashi Y, Jitsuiki D, Hara K, Kimura M, Nakagawa K, Goto C, Oshima T, Yoshizawa M, Chayama K. Smoking activates Rho-kinase in smooth muscle cells of forearm vasculature in humans. *Hypertension*. 2003;41:1102–1105.
34. Tsutamoto T, Wada A, Maeda K, Hisanaga T, Maeda Y, Fukai D, Ohnishi M, Sugimoto Y, Kinoshita M. Attenuation of compensation of endogenous cardiac natriuretic peptide system in chronic heart failure: prognostic role of plasma brain natriuretic peptide concentration in patients with chronic symptomatic left ventricular dysfunction. *Circulation*. 1997;96:509–516.
35. Creager MA, Cooke JP, Mendelsohn ME, Gallagher SJ, Coleman SM, Loscalzo J, Dzau VJ. Impaired vasodilation of forearm resistance vessels in hypercholesterolemic humans. *J Clin Invest*. 1990;86:228–234.
36. Casino PR, Kilcoyne CM, Quyyumi AA, Hoeg JM, Panza JA. The role of nitric oxide in endothelium-dependent vasodilation of hypercholesterolemic patients. *Circulation*. 1993;88:2541–2547.
37. Hattori T, Shimokawa H, Higashi M, Hiroki J, Mukai Y, Tsutsui H, Kaibuchi K, Takeshita A. Long-term inhibition of Rho-kinase suppresses left ventricular remodeling after myocardial infarction in mice. *Circulation*. 2004;109:2234–2239.
38. Curtiss C, Cohn JN, Vrobel T, Franciosa JA. Role of the renin-angiotensin system in the systemic vasoconstriction of chronic congestive heart failure. *Circulation*. 1978;58:763–770.
39. Takeshita A, Hirooka Y, Imaizumi T. Role of endothelium in control of forearm blood flow in patients with heart failure. *J Cardiac Fail*. 1996;2:S209–S215.
40. Yamakawa T, Tanaka S, Numaguchi K, Yamakawa Y, Motley ED, Ichihara S, Inagami T. Involvement of Rho-kinase in angiotensin II–induced hypertrophy of rat vascular smooth muscle cells. *Hypertension*. 2000;35:313–318.
41. Funakoshi Y, Ichiki T, Shimokawa H, Egashira K, Takeda K, Kaibuchi K, Takeya M, Yoshimura T, Takeshita A. Rho-kinase mediates angiotensin II–induced monocyte chemoattractant protein-1 expression in rat vascular smooth muscle cells. *Hypertension*. 2001;38:100–104.
42. Tekeda K, Ichiki T, Tokunou T, Iino N, Fujiki S, Kitabatake A, Shimokawa H, Takeshita A. Critical role of Rho-kinase and MEK/ERK pathways for angiotensin II–induced plasminogen activator inhibitor type-1 gene expression. *Arterioscler Thromb Vasc Biol*. 2001;21:868–873.
43. Lage SG, Kopel L, Medeiros CC, Carvalho RT, Creager MA. Angiotensin II contributes to arterial compliance in congestive heart failure. *Am J Physiol*. 2002;283:H1424–H1429.
44. Takemoto M, Sun J, Hiroki J, Shimokawa H, Liao JK. Rho-kinase mediates hypoxia-induced downregulation of endothelial nitric oxide synthase. *Circulation*. 2002;106:57–62.
45. Lee DL, Webb RC, Jin L. Hypertension and RhoA/Rho-kinase signaling in the vasculature: highlights from the recent literature. *Hypertension*. 2004;44:796–799.

Available online at www.sciencedirect.com
SCIENCE DIRECT®
Journal of Molecular and Cellular Cardiology 39 (2005) 231–239
Journal of Molecular and Cellular Cardiology
www.elsevier.com/locate/yjmcc

Original article

Contractile dysfunction of cardiomyopathic hamster myocytes is pronounced under high load conditions

Satoshi Nishimura [a], Hiroshi Yamashita [a], Masayoshi Katoh [a], Kelly P. Yamada [b], Kenji Sunagawa [c], Yasutake Saeki [d], Yosiki Ohnuki [d], Ryozo Nagai [a], Seiryo Sugiura [b,*]

[a] *The Department of Cardiovascular Medicine, Graduate School of Medicine, The University of Tokyo, Tokyo, Japan*
[b] *Computational Biomechanics Laboratory, The Institute of Environmental Studies, Graduate School of Frontier Sciences, The University of Tokyo, Hongo 7-3-1, Bunkyo-ku, Tokyo 113-0033, Japan*
[c] *The Department of Cardiovascular Medicine, Graduate School of Medicine, Kyushu University, Fukuoka, Japan*
[d] *Department of Physiology, Tsurumi University Dental School, Yokohama, Japan*

Received 12 October 2004; received in revised form 11 March 2005; accepted 30 March 2005

Available online 23 May 2005

Abstract

To understand the pathophysiology of hereditary cardiomyopathy, the contractile function of cardiomyopathic hamsters has been studied at the cellular level. However, most of the studies to date have described the cell shortening under the unloaded condition. Using a novel force–length measurement system for single cardiomyocytes, we studied the contractile function of cardiomyopathic hamster myocytes over a wide range of loading conditions. Cardiomyocytes were isolated from the ventricles of eight- to 10-week-old cardiomyopathic (CMP) hamsters (Bio TO-2 strain), as well as control (CTRL) Syrian hamsters. A pair of carbon fibers was attached to both ends of single cardiomyocytes and their contractile characteristics were recorded while changing the after-load by controlling the fiber motion. Under the unloaded condition, the shortening fraction (CMP 9.2 ± 0.5% vs. CTRL 10.7 ± 0.8%, $P = 0.06$) and maximum shortening velocity (CMP 98.2 ± 7.3 μm/s vs. CTRL 147.2 ± 6.5 μm/s, $P < 0.05$) were decreased in CMP hamster myocytes. The peak force under the isometric condition (CMP 35.8 ± 2.2 mN/mm^2 vs. CTRL 69.0 ± 8.4 mN/mm^2, $P < 0.05$) and external work (CMP 898 ± 130 J/m^3 vs. CTRL 3058 ± 576 J/m^3, $P < 0.05$) under physiologically loaded conditions were also decreased, but the differences were more pronounced under the loaded conditions. Calcium transients measured by Indo-1 revealed elevated diastolic level, decreased peak level, and slower diastolic decay in CMP myocytes thus being consistent with the observed contractile dysfunction. These results clearly indicate the importance of the loading conditions in evaluating the contractile function of CMP hamster myocytes, and may provide insights into the mechanism of contractile dysfunction in this disease.

Keywords: Cardiomyopathic hamster; Bio TO-2 strain; Cardiomyocyte; Isometric force; Calcium transient

1. Introduction

Cardiomyopathic Syrian hamsters have been used as models of hereditary cardiomyopathy and congestive heart failure. Most of the currently available strains are derived from the Bio 14.6 strain, and thus share the common genetic abnormalities identified in the exon of delta-sarcoglycan [1]. However, each strain presents a distinct phenotype depending on the stage of life. For example, some strains show significant cardiac hypertrophy in the early stage of disease (Bio 14.6, UM-X7.1 and CHF 146), whereas others (Bio 53.58 and Bio TO-2) are characterized by prominent dilation of the ventricles without wall hypertrophy [1–3].

To understand the pathogenesis of these animal models and the pathophysiology of heart failure, many studies have been undertaken at the organ [4], tissue [5,6] and cellular [7–11] levels to identify changes in the ion currents [6,11], action potentials [5], calcium kinetics [5,7,10] and mechanical properties [4,6,10]. Among these, studies on mechanics using isolated single cardiomyocytes have the advantage of establishing a direct link between subcellular abnormalities and mechanical properties by eliminating extracellular factors such as fibrosis, which is known to develop in cardiomyopathic tissue. However, most of the studies [7,10,12] in this

* Corresponding author. Tel./fax: +81 3 5841 8393.
E-mail address: sugiura@k.u-tokyo.ac.jp (S. Sugiura).

0022-2828/$ - see front matter © 2005 Elsevier Ltd. All rights reserved.
doi:10.1016/j.yjmcc.2005.03.022

field have evaluated the mechanical properties of cardiomyopathic myocytes under unloaded or light load conditions, and are far from the actual situation where the failing heart is working against high after-load and/or preload. Recently, we developed a novel force–length measurement system for isolated single cardiomyocytes using carbon fibers [13,14]. Using this system, in which the motion of the carbon fibers is controlled by a piezo-electric device, we can study the mechanics of a single cardiomyocyte over a wide range of loading conditions, including unloaded, isometric and physiologically loaded conditions.

Accordingly, the purpose of this study was to evaluate the mechanics of single cardiomyocytes isolated from cardiomyopathic hamsters (Bio TO-2 strain) in the early and compensated phases under a wide range of loading conditions. The results clearly revealed that the functional impairment became evident under high load, indicating the importance of functional analysis under loaded conditions. The underlying mechanism for the contractile dysfunction will also be discussed.

2. Materials and methods

2.1. Animals and myocyte isolation

All experiments were conducted in accordance with the National Research Council "Guide for the Care and Use of Laboratory Animals" and approved by our Institutional Animal Care and Use Committee. Eight- to 10-week-old male Syrian cardiomyopathic (CMP) hamsters (Bio TO-2 strain) and age-matched Syrian golden hamsters (control: CTRL) were obtained from the Bio-Breeders Institute (Cambridge, MA). We chose to use the hamsters at this relatively young age because Bio TO-2 strain hamsters are known to show cardiac dysfunction (low cardiac output) at this stage of life without developing significant interstitial fibrosis. The influence of fibrosis on myocyte isolation and functional analysis will be discussed later (Section 4.1).

The hamsters were anesthetized with an intraperitoneal injection of pentobarbital (500 mg/kg body wt.). After anticoagulation with heparin (10,000 U/kg i.p.) the heart was quickly removed and retrograde perfusion was initiated with nominally Ca^{2+}-free HEPES-Tyrode solution (130 mM NaCl, 5.4 mM KCl, 0.5 mM $MgCl_2$, 0.33 mM NaH_2PO_4, 22 mM glucose, 5 mM glutamine, 0.4 mM EGTA, 25 mM HEPES, pH 7.4) at 37 °C. After 5 min, the perfusate was switched to an enzyme solution containing collagenase (1 mg/ml Collagenase Type 2; Worthington), protease (0.05 mg/ml Type XIV; Sigma) and trypsin (0.05 mg/ml; Sigma) and maintained for 20 min. Finally, the enzyme was washed out by perfusion and the calcium concentration of the Tyrode solution was gradually increased to 1.1 mM. The isolated myocytes were then transferred to an experimental chamber, the glass bottom of which was coated with poly-HEME (2-hydroxyethyl methacrylate; Sigma) to prevent adhesion of the myocytes during the force and length measurements.

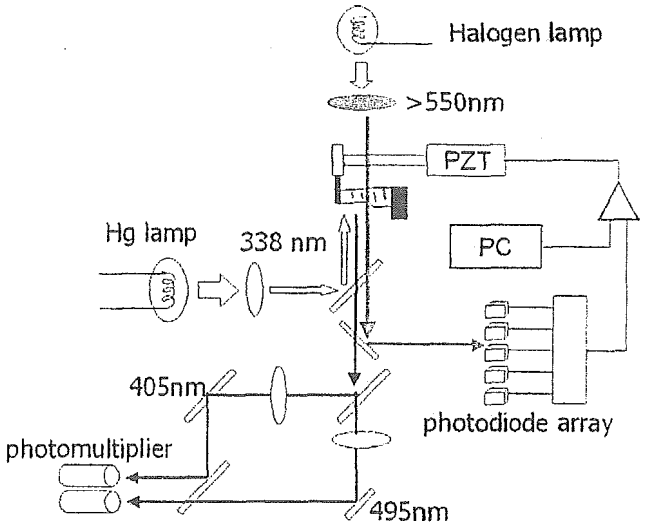

Fig. 1. Diagram of the experimental setup. The position of the fiber is detected by a photodiode array. The position signal is processed by a PC, and the calculated command signal is applied to a piezo-electric translator (PZT) connected to the carbon fiber. To observe the ratiometric Indo-1 signal, the myocytes are illuminated by a high-pressure mercury-arc lamp (excitation 338 nm) and the fluorescent light is divided by a dichroic beam splitter in order to measure two peaks of fluorescence (405 and 495 nm) simultaneously using two photomultiplier tubes.

2.2. Measurement of the force and length relationships

The principle of the single cardiomyocyte force–length measurement system has been described previously [13–15]. Briefly, a single cardiomyocyte was selected under a microscope according to the following criteria: 1) a rod shape with an average sarcomere length of > 1.65 μm (measured by on-line Fourier analysis of optical density traces of the sarcomere pattern of the myocyte image; SarcLen, IonOptix, Milton, MA); and 2) greater than 5% contraction of the total myocyte length in response to electrical stimulation. Next, a pair of carbon fibers was attached to each end of the selected myocyte using micromanipulators. One of the fibers was thin and compliant (diameter 7 μm, stiffness 80–200 nN/μm), while the other was thick and rigid (diameter 30 μm, stiffness > 1000 nN/μm) and served as a mechanical anchor. The image of the compliant fiber was projected onto a linear 1024-element photodiode array (S3903; Hamamatsu Photonics, Japan) to monitor the bending motion induced by active contraction or passive stretching (Fig. 1). Furthermore, we controlled the position of the compliant fiber by moving a piezo-electric translator (PZT) (P-841.40; Physik Instrumente, Germany) that was connected to it. Myocyte length signals obtained by the photodiode array sensor were sampled and processed at 1 kHz, and the generated command signal was applied to the PZT driver with a 16 bit A/D, D/A converter (6035E; National Instruments, TX) connected to a personal computer (PC). The myocyte was electrically stimulated at 0.5 Hz with pulses of 10 ms duration. Before the force measurements, we stretched the diastolic myocyte length to 105% of the slack length while measuring the sarcomere length (IonOptix). All experiments were performed at 37 °C (Thermo-

plate; TOKAIHIT, Japan). By controlling the motion of the PZT with the adaptive control system, we measured the contractile function under isometric, unloaded and physiologically loaded conditions in each myocyte. The cross-sectional area of the myocyte was estimated from videotaped images assuming an elliptical cross-section with a long-to-short axis ratio of 1:3.

2.3. Ca^{2+} transients

To record intracellular calcium transients, myocytes were incubated at room temperature in culture medium containing Indo-1-AM (1 μM; Wako, Japan) and Pluronic F127 (0.004%; Sigma) for 15 min. The myocytes were illuminated via epifluorescence optics (40× objective; UPlan Apo, Olympus, Tokyo) using a high-pressure mercury-arc lamp (excitation 338 nm) and the fluorescent light was divided by a dichroic beam splitter to permit simultaneous measurement of two peaks of Indo-1 fluorescence (405 and 495 nm) using two separate photomultiplier tubes. The myocytes were paced at 0.5 Hz. After confirming the stability in fluorescent signals of calcium transients (usually 5–10 s), the $[Ca^{2+}]_i$ was recorded. The data were averaged for consecutive two beats. After measurement of the intracellular calcium transients, the myocytes were permeabilized to Ca^{2+} by treatment with 25 μM digitonin (Sigma) under zero Ca^{2+} (10 mM EGTA) or 1 mM Ca^{2+} conditions to obtain the calibration factors R_{min}, R_{max} and beta. From these values $[Ca^{2+}]_i$ was calculated by $[Ca^{2+}]_i = K_d[(R - R_{min})/(R_{max} - R)]$ beta, using $K_d = 250$ nM as described in Ref. [16].

2.4. Myosin isoforms

The myosin isoform distributions of the right and left ventricular tissues from both CMP and CTRL hamsters were determined by pyrophosphate gel electrophoresis according to Martin et al. [17]. Myocardial tissue was obtained during the course of myocyte isolation, and then quickly frozen at −85 °C and thawed before processing. For each sample, equal amounts of tissue were homogenized and loaded onto the gel. After staining, the gels were analyzed using a scanning densitometer (LKB 2202; LKB Produkter, Sweden).

2.5. Data analysis

All the data were sampled at 1 kHz and recorded by an A/D converter connected to a PC (MacLab 8s; ADInstruments, Australia). The results are expressed as mean ± S.E.M., and differences between CMP and CTRL were tested for statistical significance by Student's *t*-test for unpaired data. *P* values < 0.05 were considered significant.

3. Results

3.1. Myocyte isolation and morphology

Although not significant, we observed interstitial fibrosis in the CMP ventricular tissue, which may have influenced the isolation procedure. However, we were able to collect myocytes from both CMP and CTRL ventricles with equally good viability, i.e. 90% of the myocytes were rod-shaped and responded stably to electrical stimulation. From these observations, we considered that there was no selection bias in the isolation procedure.

There were no obvious morphological differences between the cardiomyocytes isolated from CMP and CTRL hamsters (data not shown), except for the significantly shorter diastolic sarcomere length of CMP myocytes (CMP 1.72 ± 0.03 μm vs. CTRL 1.90 ± 0.02 μm, $P < 0.05$). We did not observe any width difference between the myocytes, in contrast to previous reports [10,18,19].

3.2. Force and length relationships

Eleven control myocytes and 10 cardiomyopathic myocytes were studied (Table 1). For each myocyte, we recorded the force–length relationships under a wide range of loading conditions, including isometric, unloaded and physiologically loaded conditions. A series of the force–length loops obtained under a wide range of loading conditions are shown for single myocytes from CTRL (Fig. 2A) and CMP (Fig. 2B) hamsters.

Under the unloaded condition, CMP myocytes shortened by 9.2 ± 0.5% of the myocyte length, which was lower than that for CTRL myocytes (10.7 ± 0.8%, $P = 0.06$), but the difference did not reach statistically significant. Similarly, the maximal shortening velocity (V_{max}) was significantly lower in CMP myocytes (CMP 98.2 ± 7.3 μm/s vs. CTRL 147.2 ± 6.5 μm/s, $P < 0.05$) (Table 1 and Fig. 3).

Fig. 4 shows time courses of the force (Fig. 4A) and length (Fig. 4B) changes of CTRL (solid line) and CMP (broken line) myocytes under the isometric condition. The length change was less than 0.5 μm for both groups. On average, the peak force of CTRL myocytes was 5.40 ± 0.64 μN (69.0 ± 8.4 mN/mm^2 for the cross-sectional area), which was comparable to the previously reported values for single rat ventricular myocytes [14,20,21] and papillary muscle preparations [5,6,22]. In CMP myocytes, the peak force was significantly decreased to 3.22 ± 0.24 μN (35.8 ± 2.2 mN/mm^2, $P < 0.05$). The relative reduction in the peak force was 48.0% compared to the CTRL value, and thus far greater than the relative reduction in the contractile indices obtained under the unloaded condition (shortening fraction 14.0%, V_{max} 33.3%) (Fig. 3A–C). We also found that the time course of contraction under the unloaded condition was significantly prolonged in CMP myocytes (time to half relaxation: CMP 41.5 ± 2.9 ms vs. CTRL 32.3 ± 2.7 ms, $P < 0.05$.)

When we simulated a physiological working condition consisting of isometric contraction followed by shortening and isometric relaxation (Fig. 2A, B), the average external work outputs calculated as the area circumscribed by the force–length loop were 898 ± 130 J/m^3 for CMP myocytes and 3058 ± 576 J/m^3 for CTRL myocytes. In this analysis, the difference in performance between the two groups was further accentuated (70.6% relative reduction) (Fig. 3D).

Table 1
Contractile functions of control and cardiomyopathic hamster myocytes under unloaded, isometric and physiologically loaded conditions

Control	Shortening under unloaded conditions			Force under isometric conditions		Physiologically loaded conditions		
	Length (%)	Vmax (μm/s)	RT1/2 (ms)	Force (μN)	Force (mN/mm2)	Work area (J/m2)	Slope of linear regression (nN/μm)	Sarcomere length (μm)
1	12.4	174	34	7.00	89.1	2629	1053	1.81
2	12.3	173	47	9.72	68.6	3088	2975	1.78
3	8.7	136	40	5.68	55.3	2420	1701	1.84
4	10.0	130	27	6.20	115.0	6791	2596	1.95
5	9.2	121	20	6.15	36.9	1132	1530	1.78
6	16.0	153	34	4.73	53.9	3005	797	2.01
7	12.1	173	35	3.51	50.2			1.93
8	10.0	123	28	2.76	59.0			1.96
9	7.8	139	37	3.90	52.6			1.98
10						2890		1.88
11	8.8	150	21	4.37	109.0	2506	647	1.94
Mean	10.7	147.2	32.3	5.40	69.0	3058	1614	1.90
S.E.M.	0.8	6.5	2.7	0.64	8.4	576	336	0.02
Cardiomyopathic hamsters								
1	7.8	99	38	4.04	34.0	312	314	1.66
2	9.1	81	42	2.34	40.6	1555	500	1.89
3	10.0	100	37	3.68	44.3	844	1041	1.67
4	10.8	121	63	2.16	40.1	716	398	1.67
5	11.2	136	41	4.16	40.5	1220	793	1.68
6	10.8	83	35	2.99	38.0	1169	525	1.83
7	6.3	60	41	2.71	30.8	367	659	1.73
8	7.8	119	50	4.15	30.6	1215	974	1.66
9	8.6	105	29	3.24	39.0	1053	662	1.67
10	10.1	78	39	2.73	20.1	534	593	1.73
Mean	9.2	98.2	41.5	3.22	35.8	898	646	1.72
S.E.M.	0.5	7.3	2.9	0.24	2.2	130	74	0.03

In a previous report, we showed that the curve connecting the upper left corners of force–length loops obtained under a wide range of loading conditions shifted upward and left in response to positive inotropic interventions, analogous to the end–systolic pressure–volume relationship in the rodent ventricle [14]. Applying linear regression to these points yielded slopes of 646 ± 74 nN/μm in CMP myocytes and 1614 ± 336 nN/μm in CTRL myocytes. The difference between the slopes for CMP and CTRL was also statistically significant ($P < 0.05$), thus confirming the depressed contractility of CMP myocytes.

In four myocytes for both CTRL and CMP, we measured the passive force–sarcomere–length relations as shown in Fig. 5A. Acquired curves were fitted to the following exponential function, $y = e^{\frac{x-a}{b}} - 1$, where b characterizes the curvature. We found that the constant a was significantly different between CMP (1.72 ± 0.01 μm, $n = 4$), and CTRL (1.87 ± 0.02 μm, $n = 4$), ($P > 0.05$), whereas constant b was not (CMP 0.081 ± 0.014, $n = 4$, and CTRL 0.058 ± 0.008, $n = 4$, $P = 0.10$). To elucidate the cause of this leftward shift in passive force–sarcomere–length relation, we repeated the

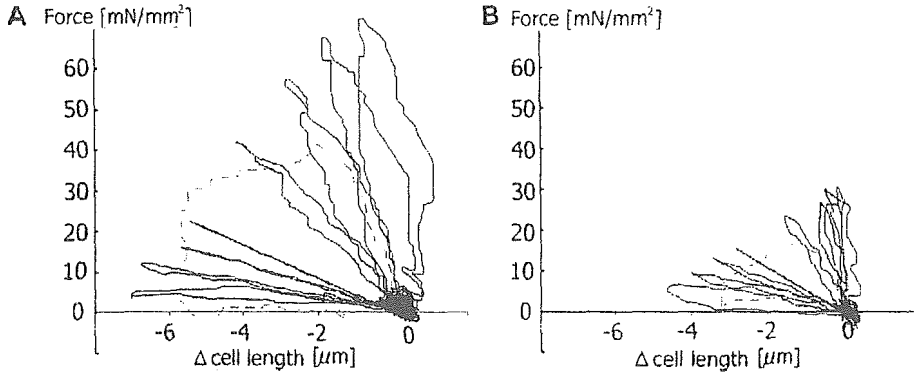

Fig. 2. Force–length loops of single cardiomyocytes under various loading conditions. Data for control (A) and CMP (B) hamster myocytes are shown. The ordinate shows myocyte length, and the abscissa shows force per cross-sectional area. In each panel, the broken line shows the loop under physiologically loaded conditions.

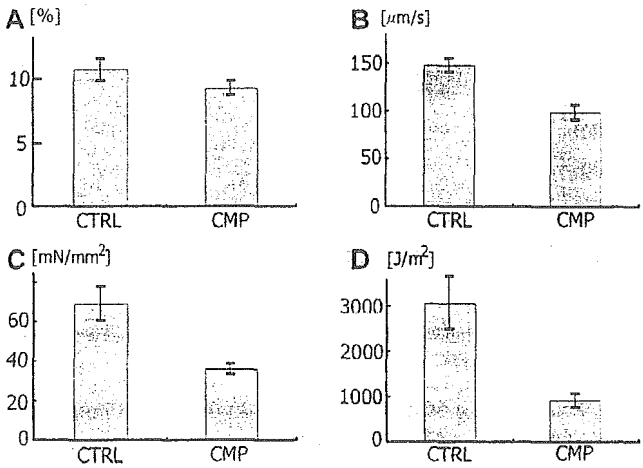

Fig. 3. Comparison of the contractile function between CMP and CTRL hamster myocytes. The shortening fraction (A) and velocity (B) under unloaded condition, isometric force (C) under isometric, and external work (D) under physiologically unloaded condition are shown. The values are mean ± S.E.M.

measurement for another three CMP and three CTRL myocytes in the presence of 20 mM 2,3-butanedione monoxime (BDM) (WAKO Chemicals, Japan) which is known to inhibit crossbridge formation [23]. Addition of BDM shifted the force–sarcomere–length relations of CMP myocytes rightward thereby made them close to those of CTRL (Fig. 5B) (CMP: $a = 1.86 \pm 0.03$ μm, $b = 0.077 \pm 0.016$, $n = 3$, CTRL: $a = 1.86 \pm 0.03$ μm, $b = 0.097 \pm 0.007$, $n = 3$).

3.3. Calcium transients

Fig. 6 shows recordings of $[Ca^{2+}]_i$ for CTRL (Fig. 6A, $n = 10$), and CMP (Fig. 6B, $n = 9$) myocyte. The peak calcium concentration was decreased in CMP cells (CMP 630.1 ± 60.6 nM vs. CTRL 805.5 ± 67.0 nM, $P < 0.05$), but the diastolic level increased (CMP 181.9 ± 32.4 nM vs. CTRL 113.4 ± 56.4 nM, $P < 0.05$). The time courses of intracellular Ca^{2+} transients were prolonged in CMP myocytes. In particular, the rate of diastolic $[Ca^{2+}]_i$ decay, as measured by the relaxation time required for half decay (RT1/2), was significantly slower in CMP myocytes (CMP 216.2 ± 13.3 ms vs. CTRL 117.1 ± 4.4 ms, $P < 0.05$).

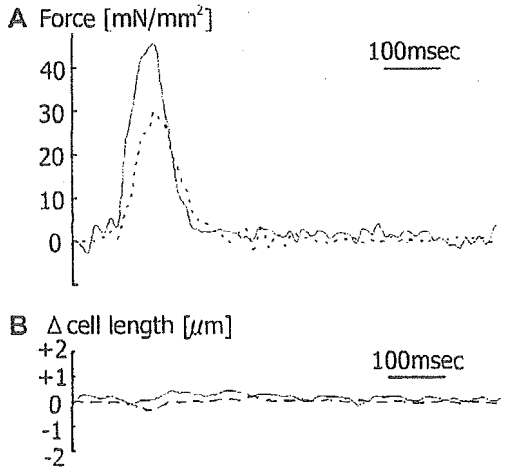

Fig. 4. Time courses of isometric contraction. Force (A) and length (B) changes for CMP (broken line) and CTRL (solid line) myocytes under the isometric condition are shown. Under the isometric condition, the length changes are less than 0.5 μm for both groups.

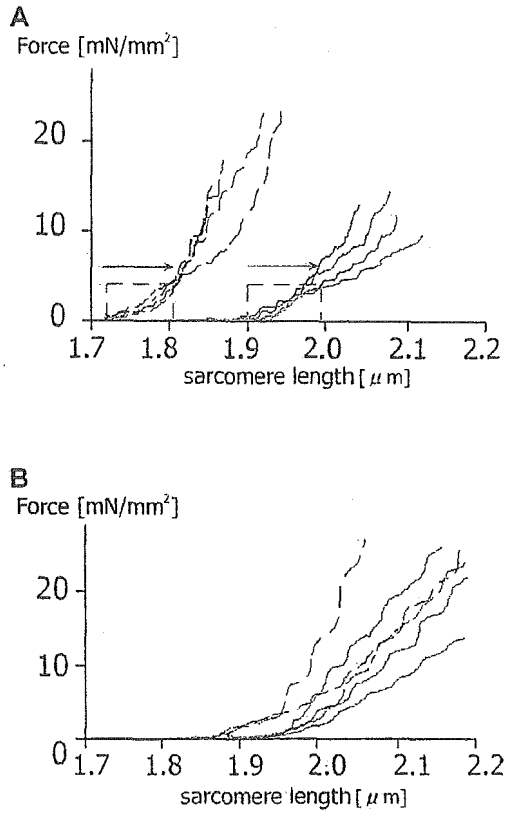

Fig. 5. A: Passive force-sarcomere length relations of CMP (broken line, $n = 4$) and CTRL (solid line, $n = 4$) myocytes. Stretching the cell to 105% of resting length (arrows and horizontal gray dotted lines) produced the same preload for both myocytes (vertical gray dotted lines). B: Passive force–sarcomere–length relations of CMP (broken line) and CTRL (solid line) myocytes in the presence of 20 mM BDM. BDM shifted the relations of CMP myocytes rightward to make them similar to those of CTRL.

3.4. Myosin isoforms

Ventricular myosin from CTRL hamsters showed a V_1 isoform predominance, whereas that from CMP hamsters showed a redistribution to V_2 and V_3 (Fig. 7) in both the left and right ventricles. When we quantified the isoform distribution by measuring the area under each peak and calculating the percentage of the α-myosin heavy chain (%α-MHC) using the formula $\%\alpha\text{-MHC} = \%V_1 + \%V_2/2$, the value was 66.3 ± 3.6% ($n = 3$) for CMP left ventricular myosin compared to 100% ($n = 3$) for CTRL.

4. Discussion

4.1. Selection of animal strain and age

In this study, we analyzed the contractile performance of single cardiomyocytes isolated from the cardiomyopathic

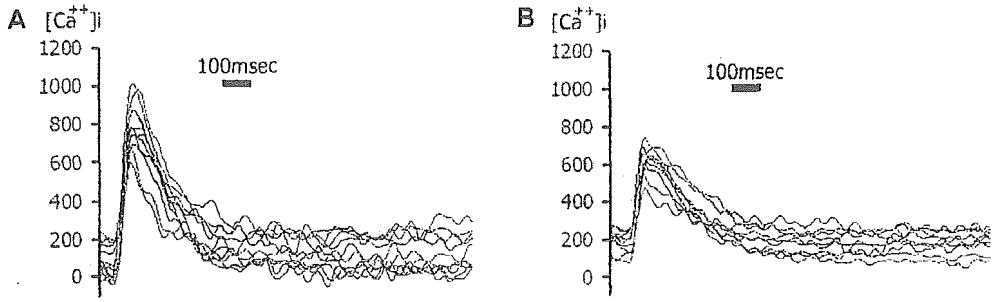

Fig. 6. Calcium transients of control (A, $n = 10$) and cardiomyopathic (B, $n = 9$) hamster myocytes calculated from the Indo-1 signal (see text for detail). The transient of CMP myocytes showed an elevated diastolic level, lower peak level, and slower diastolic decay.

hamster Bio TO-2 strain. Derived from the Bio 14.6 strain, a well-known animal model of hypertrophic cardiomyopathy, the Bio TO-2 strain shares a common defect in a gene for delta-sarcoglycan with the Bio 14.6 strain, but presents a distinct phenotype of dilated cardiomyopathy [24,25]. This difference in phenotype can be explained by the recent findings that the Bio 14.6 strain shows heterogeneously preserved alpha- and gamma-sarcoglycan with loss of beta- and delta-sarcoglycan, while Bio TO-2 strain hamsters do not show any sarcoglycans.

We selected the Bio TO-2 strain because this strain is relatively homogeneous in its clinical course, and the decrease in cardiac function (low cardiac output) starts earlier than the development of overt signs of congestive heart failure [4,6]. Furthermore, we chose to use 8-week-old hamsters, which are younger than those used in earlier studies (approximately 4 months–1 year) [7,9,10,18]. We chose this age because: 1) we may be able to detect early changes in function that are hardly modified by the compensatory mechanisms; and 2) we wanted to avoid any problems associated with cell isolation, since cardiomyopathic hamsters develop significant cardiac fibrosis which sometimes requires larger doses of proteases and longer incubation causing damage to the myocytes. Damaged myocytes tend to have calcium overload, as evidenced by their short sarcomere length, irregular shape and irritability, which may have an effect on comparisons with CTRL myocytes that are easily isolated and therefore less damaged. In many preliminary experiments, we identified the critical age limit for avoiding cell damage during the isolation procedure to be about 8 weeks. At this age, we succeeded in isolating over 90% viable (not damaged) myocytes from both CTRL and CMP hamsters.

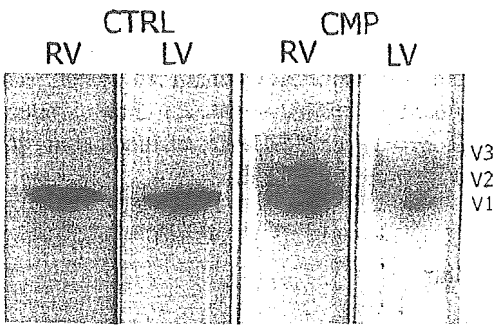

Fig. 7. Cardiac myosin isoforms. Pyrophosphate gels of cardiac myosin from the right ventricle (RV) and left ventricle (LV) of CTRL and CMP hamsters are shown. A redistribution from V_1 to V_2 and V_3 is observed in CMP myocytes.

4.2. Effect of load on performance

Using the novel force–length measurement system, we could evaluate the contractile function of single cardiomyocytes from CMP and CTRL hamsters over a wide range of loading conditions, including unloaded, isometric and physiological loading conditions.

Under the unloaded condition, we found a small difference in the shortening fraction and maximum shortening velocity between the two groups. There are only a few previous studies in which the shortening velocity and/or shortening fraction of single cardiomyocytes isolated from cardiomyopathic hamsters (Bio 14.6, CHF 146) have been discussed [7,9,10,12]. All of these studies unanimously showed a slower time course for contraction in cardiomyopathic hamsters, compatible with our results. Furthermore, the shortening fraction tended to be decreased in cardiomyopathic myocytes, although the differences were small under a low extracellular calcium concentration, also compatible with the present results.

To our knowledge, no data are available regarding the isometric twitch force for single cardiomyocytes from either normal or cardiomyopathic hamsters. However, since failing hearts are working against a high after-load in situ, evaluation of the contractile function under high load conditions is of great importance. Indeed, when we compared the isometric twitch forces of single cardiomyocytes from CTRL and CMP hamsters, we found that the difference in function was pronounced under high load conditions compared to the unloaded condition. A similar tendency was reported in a study using papillary muscle preparations, which showed a decreased tension-generating ability with a relatively maintained shortening velocity of the cardiomyopathic Syrian hamster myocardium [5]. Also in vivo condition, decreased mean arterial pressure and stroke volume have been reported for TO-2 hamsters [4]. The implications of these findings are twofold. First, the cardiomyopathic myocytes in congestive heart failure fail to match the high after-load and deteriorate further. Second, the subcellular mechanisms related to force generation may constitute the primary defect in this disease condition.

4.3. Mechanistic considerations

To gain insights into the mechanism of contractile dysfunction, we measured the calcium transients in both CTRL and CMP hamster myocytes. The results in previous reports have been conflicting. Hatem et al. [7] reported that the magnitudes of the peak intracellular calcium transients were similar between control and cardiomyopathic hamster myocytes, but the time courses were slower in the cardiomyopathic myocytes. Kruger et al. [18] reported significantly decreased peak calcium transients, whereas Sen et al. [10] reported higher time-averaged $[Ca^{2+}]_i$. Although the cause of these discrepancies is not clear, we consider that the distinct phenotype (various degree of cardiac hypertrophy or dilation) due to the different age and strain used in each study is an important factor. Our experiments were performed using younger (8 weeks of age) TO-2 strain compared to the previous reports using older (7–14 months of age) Bio 14.6 strain. The other possibility is the effect of temperature, since the experiments were performed at 37 °C in the current study and Sen et al. [10], 35 °C in Kruger et al. [18] and room temperature in Hatem et al. [7]. In this study, we observed the elevated diastolic level, decreased peak level, and slower diastolic decay of calcium transient in CMP myocytes. These changes in calcium transient were probably caused by the impairment of the sarcoplasmic reticulum function and could account for, at least in part, the shorter resting sarcomere length and impaired contractile function of CMP myocytes.

We also analyzed the myosin isoform distribution and found a shift from V_1 to V_2 and V_3 as reported in other cardiomyopathic strains [26,27]. The relationship between the myosin isoform composition and the maximum shortening velocity (V_{max}) has been studied extensively at the muscle [28,29], cellular [30] and molecular [31] levels. Using an in vitro motility assay technique, we showed that the sliding velocity of beads coated with myosin from CMP (Bio 14.6) hamster ventricles was dependent on the α-MHC content (%α-MHC) [32]. Consistent with that result, we found that the V_{max} of CMP myocytes with 66.3% α-MHC was about 70% of that of CTRL myocytes with 100% α-MHC in this study.

On the other hand, the influence of the myosin isoform redistribution on the force-generating ability of cardiac muscle is controversial and data are available only for other animal species. Using an in vitro force measurement system, VanBuren et al. [33] reported that V_3 myosin generated a greater force than V_1 myosin from rabbit, whereas Sugiura et al. [34] showed that the two myosins from rat had equal force-generating ability using a similar experimental system. The two myosins have also been suggested to have equal force-generating ability in rat papillary muscle preparations [35]. However, these results cannot add much to the explanation for the smaller force observed in the CMP hamster myocytes containing a greater amount of the V_3 myosin isoform.

Recent studies have identified mutations in the exon of delta-sarcoglycan in cardiomyopathic hamsters [1,36]. Since sarcoglycans are located in the sarcolemma as anchors connecting myofibrillar proteins to the sarcolemma via cytoskeletal proteins [37], abnormalities in these proteins can cause defects in transmission of the force generated by the contractile proteins to the extracellular matrix. The present finding that the contractile dysfunction of Bio TO-2 hamster myocytes is pronounced under high load may provide support for this hypothesis, although further studies are required to fully address this issue.

We also found that the passive force–sarcomere–length relations of cardiomyopathic myocytes were shifted leftward compared to the control indicating the stiffer passive property. We consider the crossbridge formation due to the elevated diastolic calcium level to be the major cause. Normalization of leftward shift by the BDM in cardiomyopathic myocytes strongly supported this hypothesis, but other factors should also be taken into account. We can find a paper reporting the stiff passive property of cardiomyopathic papillary muscle [5]. Although direct comparison was difficult, because sarcomere length was not measured in their study, passive property of our control myocytes were close to their control one. On the other hand, passive property of cardiomyopathic myocytes was stiffer compared to papillary muscle data. Extracellular collagen mesh exists in multi-cellular preparation but, as shown by Granzier and Irving [38], its contribution to the passive property is minimal in the short sarcomere length studied here. Alternatively, we speculate the other role of collagen mesh in modulating the experimentally determined passive property. In papillary muscle preparations, with the aid of collagen mesh, tensile stress applied at the ends could be distributed homogeneously over the sarcolemma and transmitted to each sarcomere through costameres. On the other hand, sarcomeres might not be stretched efficiently in cardiomyocyte by the force applied and concentrated at the edge of sarcolemma. In addition, as stated above, the defects in delta-sarcoglycan could impair the force transmission to sarcomere in CMP myocytes. In fact, loosening sarcomeres has been reported in the absence of cytoskeletal protein desmin connecting the Z-line in skeletal muscle [39].

In this study, comparison of contractile function was made at different sarcomere length between the two groups because of the following reasons. Upon isolation, resting sarcomere length was significantly shorter for CMP animals possibly due to the increased diastolic calcium concentration. Fig. 5 also shows that if we tried to stretch the sarcomere length of CMP myocytes to the same level with CTRL myocytes, it required abnormally high tension. Indeed, upon stretch of such degree, CMP myocyte contracted spontaneously probably due to the activation of stretch activated channel and hampered our measurement under steady-state condition. However, in the shorter sarcomere length range, where tension-sarcomere length relations were relatively linear and flat, so that the 5% stretch from the resting length (horizontal dotted lines in Fig. 5A) required comparable tension (preload) (vertical dotted lines in Fig. 5A) for both cases. For this reason, we made comparison at the constant preload by stretching the myocytes from both groups to 105% of resting length.